Using portable emissions measurement systems (PEMS) to derive more accurate estimates of fuel use and nitrogen oxides emissions from modern Euro 6 passenger cars under real-world driving conditions

Justin D K Bishop[a,b], N Molden[c], Adam M Boies[b]

[a] *Arup, 13 Fitzroy Street, London W1T 4BQ, United Kingdom*
[b] *Centre for Sustainable Road Freight, University of Cambridge Department of Engineering, Trumpington Street, Cambridge CB2 1PZ, United Kingdom*
[c] *Emissions Analytics, Manor Farm, Romsey Road, Pitt, Winchester, Hampshire SO22 5QX, United Kingdom*

Abstract

Data from portable emissions measurement systems (PEMS) and other sources have allowed the discrepancy between type approval and real-world fuel economy and nitrogen oxides (NO_x) emissions to be both identified and quantified. However, a gap in the knowledge persists because identifying this discrepancy does not allow us to predict real-world fuel economy and emissions accurately. We address this gap in the knowledge using a bottom-up approach: a PEMS is used across a range of Euro 6 petrol and diesel vehicles, from which internally-consistent powertrain models are derived. These training vehicles are simulated over 20 real-world and regulated driving cycles. 26 metrics representing driving, vehicle and ambient characteristics are used to develop quantile regression (QR) models for three vehicle groups: direct-injection petrol vehicles with three way catalysts; diesel vehicles with selective catalytic reduction; and diesel vehicles with lean NO_x traps. 95% prediction intervals are used to assess the predictive accuracy of the QR models from a set of validation vehicles. Across the vehicle groups, QR models for both fuel economy and NO_x emissions depended on the dynamics of the driving cycles more than the engine characteristics or ambient conditions. The 95% prediction interval for fuel economy enclosed most of the observed values from the PEMS test, with similar prediction error to COPERT in most cases. The benefits of the QR approach were more pronounced for NO_x emissions, where the majority of PEMS observed data was enclosed in the 95% PI and median prediction error was up to two times lower than COPERT.

Keywords:
On-board diagnostics (OBD), Engine maps, Vehicle powertrain modelling, Emissions, Portable emissions measurement systems (PEMS)

Email address: justin.bishop@cantab.net (Justin D K Bishop)

1. Introduction

The objective of this paper is to derive new, closed-form equations for fuel economy and nitrogen oxides (NO_x) emissions from Euro 6 passenger vehicles. Currently, the literature has focused on the discrepancy between type approval tests and real-world driving for fuel economy and emissions. Both identifying and quantifying this gap has helped to expand the type approval procedure in Europe to include a Real Driving Emissions (RDE) test [1]. However, knowing the size of the discrepancy does not allow us to make more accurate predictions of real-world fuel economy and emissions. We address this gap in the knowledge using data from Euro 6 passenger vehicles equipped with portable emissions measurement systems (PEMS) tested in the UK.

Type approval test results suggest new car average carbon dioxide (CO_2) emissions in the European Union was 126.7 g CO_2/km in 2013, meeting the 2015 target of 130 g CO_2/km [2] two years early. Provisional data suggests new car average CO_2 emissions were 118.1 g/km at the end of 2016 [3]. However, real-world testing shows CO_2 emissions from new vehicles in were 39% higher than their type approval values in 2017 [4], down from a peak of 42% in 2015 [5] and 2016 [6]. In 2017, the market share of diesel vehicles fell to 45% across Europe, while petrol vehicle market share rose to 49%. This is the first time that petrol vehicles outsold diesels since 2009 [7]. The combination of a shift to petrol vehicles and low penetration (1.5%) of zero tailpipe emissions vehicles led to average new car CO_2 emissions increasing by 0.4% to 118.5 g/km in 2017 [8].

Likewise, since 2014, passenger vehicles entering service should meet the latest Euro 6 standards of 0.06 g NO_x/km for petrols and 0.08 g NO_x/km for diesels [9]. However, real-world NO_x emissions from Euro 6 diesel vehicles were on average 4.5 times higher than the regulatory limits, ranging from those which meet the emissions standard to those which exceed it by 12 times [10]. At this level, the average modern diesel vehicles fail even to meet the Euro 4 standards introduced in January 2005, implying average real-world emissions have not improved in the decade to 2017. Indeed, emissions arising from driving behaviour similar to that used for type approval showed little overlap with emissions achieved under a controlled lab setting, even after accounting for ambient conditions. This discrepancy has been attributed to the modification of emissions control strategies during certification testing and implies the use of defeat devices [11]. Consequently, progress towards lower emissions of both CO_2 and local air pollutants envisioned by European legislation has not been realised fully.

Emissions are influenced by the characteristics of a vehicle, how it is driven and external environmental conditions. Currently, emissions factors within the Computer Programme to calculate Emissions from Road Transport (COPERT) v5 are used to generate emissions inventories in Europe. COPERT is based on the efforts described in the Handbook Emissions Factors for Road Transport (HBEFA). Here, 20 first generation (1 petrol, 19 diesel) Euro 6 vehicles were tested on a dynamometer over the New European

Driving Cycle (NEDC) and the Common Artemis Driving Cycle (CADC) representing the regulated test cycle and real-world driving, respectively [12]. A recent update of HBEFA includes data from 25 model year 2014-2015 Euro 6 diesel vehicles equipped with PEMS operating under real-world conditions [13]. The HBEFA approach does not produce vehicle specific engine maps for fuel use: instead, a generic CO_2 engine map and a correction factor are used to account for the technological improvements in modern engines. Measured engine speed and CO_2 emissions from the PEMS tests are used to estimate instantaneous engine power. Maps of other emissions are created using the estimated engine power and observed speed. Whereas HBEFA use expected technological progress to predict fuel economy and emissions of later Euro 6 vehicles, we use PEMS data to develop engine maps specific to vehicle. Therefore, our maps and subsequent emissions factors internalise actual technological progress because they are based on vehicles in service from model year 2014 onwards. Finally, HBEFA compresses the engine maps of individual vehicles into a sales-weighted, normalised equivalent to simulate the vehicles across a range of other driving cycles to derive the closed form emissions factors for COPERT. These COPERT Euro 6 emissions factors are average-speed based, defined only above 5 km/h for petrol and 10 km/h for diesel and classified only by fuel type.

Recent investigations suggest additional vehicle parameters and driving style metrics influence real-world fuel economy and emissions. Positive kinetic energy, relative positive acceleration (RPA) and root mean squared (RMS) acceleration influenced emissions from four petrol Euro 4 passenger cars with similar engine sizes tested in India [14]. RPA is given by $\sum_{i=1}^{n} \frac{a_i \cdot v_i}{3.6}/dist$ for all accelerations $a_i > 0$ and is one measure used to represent the dynamics of a driving cycle [15]. RPA, the 95^{th} percentile of the product of velocity and acceleration and mean positive acceleration were used to evaluate a Euro 5 and a Euro 6 vehicle, both equipped with diesel oxidation catalysts (DOC) on routes meeting the RDE specifications [16]. RPA and the number of accelerations and decelerations influenced NO_x emissions most for a Euro 6 diesel passenger car equipped with a PEMS in Spain [17]. A simple regression of observed fuel economy as a function of type approval fuel economy, mass and engine capacity [18] was extended to include model year [19]. Six Euro 6 diesel passenger cars with lean NO_x traps were tested over two routes in Korea using a PEMS [20]. Here, ambient temperature was found to be important in trip-level NO_x emissions because exhaust gas recirculation (EGR) was stopped to prevent damage to the filter from moist particulate matter in the exhaust stream. A separate study of 39 passenger cars (17 Euro 6) found ambient temperature influenced selective catalytic reduction (SCR) technologies also [21]. Engine-out NO_x content, storage capacity of the LNT, vehicle driving patterns and ambient temperature were found to influence NO_x control schemes on a 2016 2.2 litre diesel engine [22].

A number of works have applied an approach similar to MOVES (activity-weighted, vehicle specific power (VSP)) to assess emissions from European vehicles. Often, 'typical' values of drag coefficient (C_d) and frontal area are used to describe the full range of vehicle sizes, from mini to sport utility and multi-purpose vehicles. The MOVES documentation admits to maintaining constant road load parameters in their

methodology, even if they are not representative in the real-world [23]. A VSP-approach with 14 bins was used for 16 Euro 5 vehicles equipped with PEMS [24] and 25 bins were used in the multivariate analysis on 14 petrol passenger cars with PEMS [25]. In this latter work, the low correlation coefficients ($R^2 \leq 0.78$) for the multivariate analysis imply NO_x production is influenced by metrics other than VSP. Higher correlation coefficients ($R^2 > 0.90$) were achieved when using VSP bins to predict CO_2 emissions in 78 diesel and petrol vehicles equipped with a PEMS [26]. However, those authors assumed all passenger cars and light-duty trucks were driven in third gear most of the time and had the same physical characteristics: $C_d = 0.3$; frontal area of 2 m^2; and mass of 1200 kg. VSP bins were populated with the results of Monte Carlo simulations to yield average emissions per bin. Fuel economy and emissions were calculated for 82 vehicles and 23 bins, assuming typical MOVES VSP coefficients [27]. Large differences in fuel economy and emissions were observed with changes in driving style. In contrast, the method used in this work calculates the likely physical characteristics for each vehicle. Moreover, our VSP metric incorporates the instantaneous road grade which is not included in MOVES [28].

Another activity-weighted approach is the moving average window (MAW) with RPA for 12 Euro 5 vehicles in Korea [29]. NO_x emissions were different under comparable operating conditions if the driving cycles were different, implying cycle-specific emissions control. In many cases, emissions factors were provided for individual vehicles, but not a closed-form, general type to be used for predicting emissions more generally.

Other efforts to determine emissions factors rely on black box methods, such as artificial neural networks (ANN). An ANN was developed to predict real-time exhaust from emissions recorded using six diesel vehicles [30]. MOVES' typical VSP coefficients were used with 11 bins. Input neurons were vehicle speed, acceleration, engine speed and VSP. Including oil temperature and throttle position yielded marginal improvement in model predictive accuracy.

Finally, roadside measurement campaigns have been used to investigate the impact of driving style on vehicle emissions. VSP accounted well for the effect of driving on emissions [31]. For diesel vehicles, engine size and manufacturer were found to influence emissions of both NO_x and nitrogen dioxide.

This paper adopts a bottom-up approach to determine emissions factors based on 76 pre-RDE Euro 6 vehicles (32 petrol, 49 diesels) equipped with PEMS and tested by Emissions Analytics (EA). Vehicle road load characteristics and maps of fuel use and NO_x emissions were extracted for each vehicle [32]. The vehicles were simulated over a range of regulated and real-world driving cycles. Driving cycle metrics, vehicle characteristics and ambient conditions were used to train quantile regression (QR) models of emissions factors. A separate validation set of PEMS data was used to test the accuracy of the new emissions factors which is discussed as part of the results.

2. Method

A schematic of the method is given in Figure 1 and comprises three parts: the first extracts vehicle characteristics and engine maps of fuel use and NO_x emissions (hot); the second identifies a training set of vehicles and simulates them across 20 regulated and real-world driving cycles; and the third applies QR to a set of vehicle characteristics, driving behaviour and ambient conditions to establish closed-form emissions factors. The predictive accuracy of the new emissions factors is demonstrated using a validation set of PEMS data. This work was executed in Matlab R2018b.

Each vehicle was instrumented with a Semtech DS PEMS and driven once on a non RDE-compliant 40 km circuit west of London which comprised urban, rural and motorway driving. Tests occurred across a range of ambient conditions. Therefore, we consider average air temperature and relative humidity explicitly as predictors of fuel economy and NO_x emissions.

The engine mapper technique developed in [32] was employed in this work. In summary, the engine mapper uses data recorded from vehicles under real-world driving conditions to inform a powertrain model: First, engine speed and wheel speed data is used to determine the effective gear ratio, which internalises tyre diameter, final drive and individual transmission ratios in the gearbox. Second, a range of values of C_dA, C_{rr} and vehicle mass – initial estimates and each varying $\pm 20\%$ – are tested over the observed driving cycle to determine the combination of road load factors which yields the smallest sum of absolute deviations (SAD) per second between observed and simulated engine speed. Finally, the engine map of outputs – fuel use and emissions (where reported) – is created by classifying the distribution of output values into 2x2 boxes, 3x3 boxes and so on up to 10x10 boxes. The mean of the output values in each box is assigned to that area of the engine torque-speed map. The vehicle is simulated over the driving cycle and the number of boxes chosen which returns the smallest SAD per second between observed and simulated output.

2.1. Identify training and validation vehicles

2.1.1. Training vehicles

Vehicles with hybridised powertrains were excluded from training as the engine mapping procedure applies to conventional powertrains only [32]. Vehicles were used in the training set if simulated trip-level fuel economy and NO_x emissions were within 6% of the values observed in the PEMS test. In this work, 22 vehicles were used for training. There is a broad range of engine and exhaust after-treatment technologies used in vehicles currently. For this work, vehicles were grouped by Euro standard, fuel-air delivery method and exhaust after-treatment technology, with details in Table 1. Specifications of training vehicles can be found in Table 2. Table 3 lists the regulated and real-world driving cycles which training vehicles were simulated over. Vehicles were simulated using ADVISOR version 2003-00-r0116. The EA driving cycle which the original PEMS data was collected over is in the group of 20 cycles. However, the outputs from that cycle were not used to train the QR.

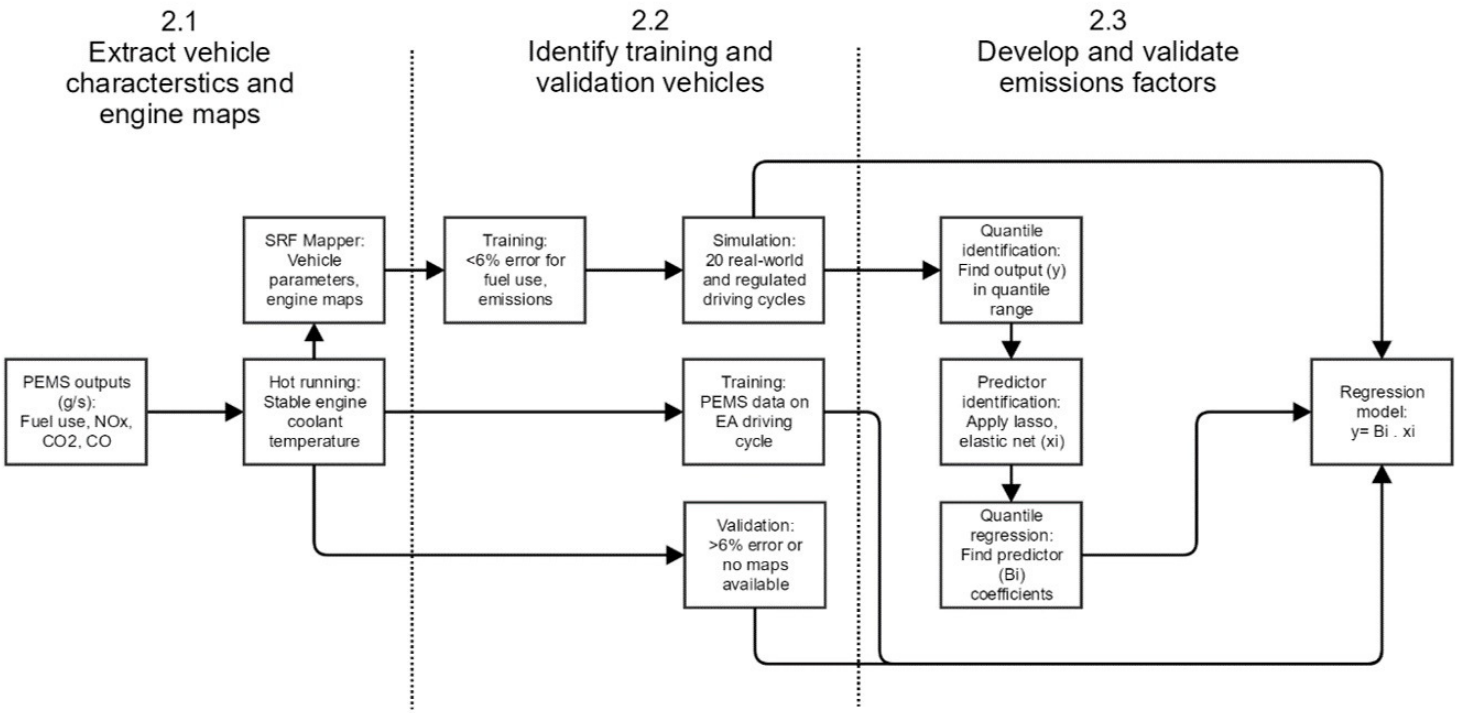

Figure 1: Schematic of method to develop and validate emissions factors from Euro 6 passenger vehicles equipped with PEMS.

Table 1: Codes for groups of vehicles by Euro standard, fuel-air delivery method and exhaust after-treatment technology. Number of turbochargers and after-treatment technology was determined from the automobile catalog (available at `https://www.automobile-catalog.com/`).

Fuel	Code	Fuel-air delivery method
Petrol	1	Port injected, spark ignition (PISI), natural aspiration
	2	PISI, turbocharged
	3	PISI, multiple turbochargers
	4	Direct injected, spark ignition (DISI), natural aspiration
	5	DISI, turbocharged
	6	DISI, multiple turbochargers
		Exhaust after-treatment technology
	6	Three way catalyst (TWC)
Diesel	7	Direct injected, compression ignition (DICI), turbocharged
	8	DICI, multiple turbochargers
		Exhaust after-treatment technology
	1	Lean NO_x trap (LNT)
	2	Exhaust gas recirculation (EGR)
	3	Selective catalytic reduction (SCR)
	4	Diesel oxidation catalyst (DOC)
	5	SCR, DOC
	7	DeNO_x, DOC
	8	LNT, DOC
	10	EGR, DOC

Table 2: Make, model and year of training vehicles, including derived vehicle characteristics, engine specifications and classification group (see Table 1). Vehicle characteristics of drag, rolling resistance and test mass derived from engine mapping and simulation procedure in [32]. Engine details taken from manufacturer data sheets.

Year	Vehicle make/model	Fuel type	C_dA (m^2)	Crr	Test mass (kg)	Peak T (Nm)	Peak P (kW)	Group
2014	Ford Ecosport	Diesel	0.7	0.00038	1370	140	82	DICI-T-DOC
2014	Seat LEON TSI	Petrol	0.6	0.00036	1277	250	110	DISI-T-TWC
2015	Volvo V40	Petrol	0.57	0.00036	1447	350	132	DISI-T-TWC
2015	Volkswagen Golf SV	Diesel	0.74	0.00044	1474	340	110	DICI-T-LNT
2016	Opel/Vauxhall Astra EliteNav SportsTourer CDTi	Diesel	0.65	0.00042	1830	320	100	DICI-T-LNT
2016	Volkswagen Passat Bluemotion TDi	Diesel	0.6	0.00042	1722	250	78	DICI-T-LNT
2016	Ford Kuga Titanium X	Petrol	0.83	0.0004	1504	240	110	DISI-T-TWC
2016	Kia Sportage 2 ISG CRDI	Diesel	0.8	0.00036	1425	280	85	DICI-T-LNT-DOC
2016	Toyota RAV4 Icon D-4D 4x2	Diesel	0.75	0.00036	1610	310	91	DICI-MT-LNT
2016	Porsche Boxster 718 S	Petrol	0.59	0.0004	1355	420	257	DISI-T-TWC
2016	Jaguar XJ R-Sport	Diesel	0.68	0.00044	1835	700	221	DICI-MT-DOC
2016	Volkswagen CC R-Line Black Edition BlueMotion Technology	Diesel	0.59	0.00042	1582	380	130	DICI-T-SCR
2016	Bentley Bentayga W12	Petrol	1.04	0.00038	2422	900	447	DISI-MT-TWC
2016	Rolls-Royce Dawn	Petrol	0.85	0.00038	2560	780	420	DISI-T-TWC
2016	Ford EcoSport Titanium TDCI	Diesel	0.82	0.00044	1384	205	66	DICI-T-DOC
2016	Seat Ibiza Cupra	Petrol	0.72	0.00044	1260	320	141	DISI-T-TWC
2016	Mazda Mazda3 Sports Line Skyactiv-D	Diesel	0.61	0.00044	1308	270	77	DICI-T-DOC
2016	Mercedes-Benz CLA-Class C 200d AMG Sport	Diesel	0.53	0.00042	1450	300	101	DICI-T-SCR-DOC
2016	Mercedes-Benz CLA-Class CLA 220d AMG Sport	Diesel	0.46	0.00036	1450	350	132	DICI-T-DOC
2016	Fiat 500L Beats Edition Multijet	Diesel	0.64	0.0004	1415	320	89	DICI-T-DOC
2016	Audi Q2 TDI Quattro	Diesel	0.79	0.00036	1550	340	110	DICI-T-SCR
2016	Infiniti Q50 Sport D	Diesel	0.61	0.00042	1696	400	125	DICI-MT-DOC

Table 3: Regulated and real-world driving cycles. The country where the driving cycle applies is given in brackets.

Driving cycle	
Regulated	Real-world
NEDC (Europe)	EA PEMS* (Europe)
HWFET (US)	Artemis (Europe)
INRETS (Europe)	Artemis urban (Europe)
LA92 (US)	TRL urban (UK)
IM240 (US)	TRL congested (UK)
UDDS (US)	HBEFA R1 (Europe)
US06 (US)	HBEFA R2 (Europe)
WLTP (World)	HBEFA R3 (Europe)
NYCC (US)	HBEFA R4 (Europe)
JC08 (Japan)	Passing (US)

26 metrics (predictors) were extracted from these driving cycles to avoid pre-supposing which may influence fuel economy and NO_x emissions significantly. The metrics were taken from the TRL handbook [15] and 11 additional parameters from the literature reviewed earlier, recognising the importance of the vehicle itself (nine metrics) and ambient conditions (two metrics) on the the quantity of emissions generated (Table 4). An inspection of the variation in fuel economy and NO_x emissions with metrics in Appendix Appendix B suggested the existence of non-linear relationships. Therefore, the base predictors, x_i, were expanded to include: $\frac{1}{x_i}$, $ln(x_i)$ and e^{x_i}.

2.1.2. Validation vehicles

There were two classes of validation vehicles. The first set comprised the 54 vehicles for which engine maps could either not be created due to missing data, such as engine speed, or were not accurate enough to reproduce trip-level fuel economy and NO_x emissions to within 6% of observed. The second validation set used the PEMS data from the 22 training vehicles, rather than the outputs of the vehicle model development and driving cycle simulations.

2.2. Develop and validate emissions factors

Achieving closed form emissions factors requires a relationship between the dependent variable (y) – fuel economy or NO_x emissions – and one or more predictors, x_i, describing the vehicle and how it is driven. QR is used in this work because it is non-parametric: the distribution of y and x can change and no assumption

Table 4: Driving cycle metrics, vehicle characteristics and ambient conditions used for training emissions factors. RMS = root mean squared; IQR = interquartile range

Driving cycle metrics
Velocity, m/s (running, median, relative positive squared, relative positive cubed, aerodynamic, IQR, maximum)
Number of accelerations-decelerations, per km
Acceleration, m/s^2 (median, maximum, RMS, relative positive, characteristic, IQR)
Deceleration, m/s^2 (median, maximum, relative negative)
Vehicle specific power, kW/kg (median, IQR, maximum)
Stops, per km
Modes, (proportion of time idling, accelerating, cruising and decelerating)
Kinematic intensity, per km
$95t^{th}$ percentile of the product of velocity and acceleration, m^2/s^3
Jolt, m/s^3 (median, IQR)
Vehicle characteristics
Torque, Nm (peak, specific (Nm/kg))
Power, kW (peak, specific (kW/kg))
Volume (engine), (absolute, specific (cc/kg))
Mass, kg
Brake mean effective pressure (BMEP) kPa, (peak, specific (kPa/kg))
Turbo code
Model year
Cylinder number
Compression ratio (median)
External variables
Ambient temperature, ℃ (median)
Relative humidity, % (median)

is made of the distribution of errors [33]:

$$y = \beta_i \cdot x_i + \epsilon \; \forall i = 1, ..., n; \tag{1}$$

where: n = number of predictors, x; and ϵ = the prediction error, the difference between the observed value (y) and the model.

The aim was to produce closed form emissions factors which predicted the test and validation data accurately, but were not over-fitted to the training data. To achieve this, the number of predictors was reduced in two steps using the Least Absolute Shrinkage and Selection Operator (lasso), with and without elastic net [33].

The lasso penalty, λ_1, is based on the absolute value of the coefficients (β) of the predictors and increases with model complexity (number of predictors):

$$L_1 = L(\beta) + \lambda_1 \sum_{i=1}^{n} |\beta_i|; \tag{2}$$

where: $L(\beta)$ is the empirical loss function of y; and λ_1 is the lasso penalty applied to the coefficient of each predictor, x_i.

Small values of lambda yield $\beta = 0$ for all predictors (constant model). As λ_1 increases, more coefficients become non-zero until all predictors are represented in the regression for sufficiently large λ_1 (unpenalised). Therefore, the lasso approach returns a set of model candidates, with number of predictors increasing with λ_1.

However, the lasso can be suboptimal for correlated predictors. A second penalty, λ_2 was introduced to form the elastic net, allowing correlated predictors to achieve non-zero β for small λ_1. The aim of the elastic net is to minimise L_2:

$$L_2 = L(\beta) + \lambda_1 \sum_{i=1}^{n} |\beta_i| + \lambda_2 \sum_{i=1}^{n} \beta_i^2; \tag{3}$$

where: λ_2 is the elastic net penalty applied to the coefficient of each predictor, x_i.

The lasso (with k=5 cross-validation) was applied to all predictors within the set of training vehicles for a chosen QR quantile (τ) of y. The model candidate was chosen with the smallest number of predictors (greater than one). The lasso (with k=5 cross-validation) and elastic net ($\lambda_2 = 0.1$) was applied to the original, full set of predictors and a new model candidate chosen as before. The QR model used the union of predictors from the lasso, with and without the elastic net across all quantiles.

This work considered the 95% prediction interval (PI) which is a region where 95% of the true study effects are expected to be found [34]. Therefore, the quantiles, τ = [0.025 0.5 0.975] were used as it was expected that predictors would have different influences depending on the quantile chosen. QR models can

cross when the predicted value of a low percentile exceeds that of a higher percentile. In this work, crossing is not explicitly controlled because of the breadth of the PI. However, non-crossing was verified in the results.

The output of the QR was the β_i for each predictor x_i in the reduced model. The training, testing and validation data were evaluated on this model at each τ quantile for different groups of vehicles from Table 1:

- all petrol vehicles with turbocharged, direct injection engines;
- all diesel vehicles using a LNT alone, or paired with a DOC; and
- all diesel vehicles using a SCR alone, or paired with other technology.

The resulting QR models adopted the form $y = \sum_{i=1}^{n} \beta \cdot x_i$ for all predictors, x_i. The outputs were compared to the training data and predictions using COPERT v5 where Emissions Factor (EF) takes the form [35]:

$$EF = \frac{\alpha \cdot v^2 + \beta \cdot v + \gamma + \frac{\delta}{v}}{\epsilon \cdot v^2 + \zeta \cdot v + \eta} \cdot (1 - RF) \tag{4}$$

Euro 6 vehicles are differentiated by year of introduction: Euro 6_1 in 2015-2016; Euro 6_2 for 2017-2019; and Euro 6_3 for 2020 onwards. In this work, we used Euro 6_1 and Euro 6_2 emissions factors for our pre-RDE vehicles because they were first registered in 2015-2017.

The coefficients of the polynomial to predict fuel economy in COPERT v5 were specific to vehicle size segment, fuel type (petrol, diesel), but not year of introduction. Within the same fuel type, the coefficients of the polynomial depended upon the vehicle size segment. In this work, we use the average value of the polynomial coefficient across vehicle size segments.

The result was two sets of polynomial coefficients: one representing all Euro 6_1 and Euro 6_2 petrol vehicles; and the other for all Euro 6_1 and Euro 6_2 diesel vehicles. For NO_x emissions, polynomial coefficients were the same across vehicle size segment, but different for fuel type and year of introduction. Therefore, four sets of polynomials were required: one for each of Euro 6_1 and 6_2 petrol; and one for each of Euro 6_1 and 6_2 diesel.

There are two main differences between the COPERT model and that proposed in this paper. First, COPERT is based on average velocity and engine size to represent the dynamics of driving and vehicle characteristics, respectively. Our QR model uses 26 predictors, with 15 representing driving dynamics, nine for the vehicle characteristics and two for external ambient conditions. Secondly, COPERT uses the polynomial form given above for fuel use and all pollutants, while the form of each of our emissions factors is derived from the QR model based on the interaction of predictors for each vehicle group.

3. Results and discussion

3.1. PEMS results by vehicle group

Figure 2 illustrates the trip-level NO_x emissions from the training and validation set of petrol and diesel vehicles. The three way catalyst (TWC) was effective at maintaining emissions within the Euro 6 limit, save for two vehicles (Figure 2a): one PISI turbo vehicle at 0.065 g/km; and one DISI turbo vehicle at 0.067 g/km.

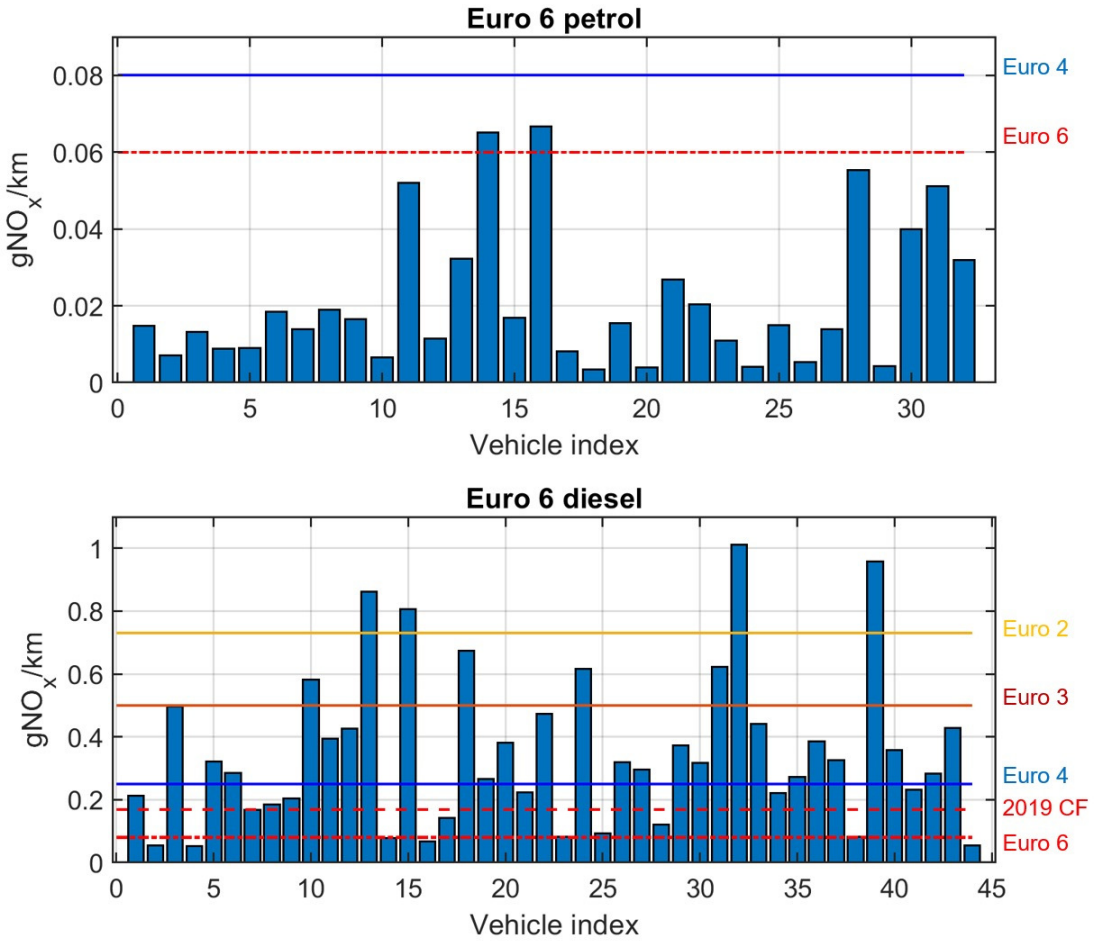

Figure 2: Bar graphs of trip-level NO_x emissions for the training and validation set of a) petrol and b) diesel vehicles. Horizontal lines indicate the NO_x limits at various Euro standards.

In contrast, most diesels exceeded both the Euro 6 emissions standards of 0.08 g/km and the 2019 conformity factor of 2.1 times the Euro standard (red broken line in Figure 2b), save five (all single turbos): two vehicles with LNT at 0.037 g/km, 0.052 g/km; one with a DOC at 0.054 g/km; one with a SCR at

0.073 g/km; and one with SCR and DOC at 0.067 g/km. Notably, three of these vehicles also met the Euro 6 petrol standard, demonstrating that modern diesel vehicles can be as clean as petrols from a NO_x emissions perspective.

Figure 3 illustrates the range of fuel economy and NO_x emissions for the petrol and diesels when grouped by fuel-air delivery method and exhaust after-treatment technology. In general, fuel economy of the petrol vehicles using port injection decreased a median 46% from 6.8 l/100 km to 9.9 l/100 km for vehicles with direct injection and multiple turbochargers. Median fuel economy for diesel vehicles was 5.7-5.8 l/100 km, except for three groups (all with multiple turbochargers): one with a SCR and DOC at 6.8 l/100 km; one with a LNT at 6.2 l/100 km; and one with a DOC only at 6.4 l/100 km.

Table 5: Median and range of fuel economy and NO_x emissions for groups of vehicles by Euro standard, fuel-air delivery method and exhaust after-treatment technology, with number of vehicles per group.

Group	Fuel economy (l/100km)	NO_x emissions (g/km)	n
PISI TWC	6.8 (6.3-7.4)	0.01 (0.0042-0.017)	2
PISI-T TWC	6.8 (6.6-7.1)	0.037 (0.0082-0.065)	2
DISI-T TWC	7.4 (5.4-16)	0.014 (0.0034-0.067)	24
DISI-MT TWC	9.9 (8.2-15)	0.026 (0.009-0.052)	4
DICI-T LNT	5.7 (5.1-9.7)	0.43 (0.036-1.1)	9
DICI-T SCR	5.8 (4.9-6.2)	0.27 (0.073-0.38)	5
DICI-T DOC	5.6 (5.3-8)	0.25 (0.054-0.82)	14
DICI-T SCR-DOC	5.5 (5.3-7.7)	0.26 (0.067-0.39)	6
DICI-T LNT-DOC	5.5 (5.3-5.6)	0.64 (0.32-0.96)	2
DICI-MT LNT	6.2 (5.7-7.7)	0.41 (0.29-0.62)	3
DICI-MT DOC	6.4 (5-7.5)	0.25 (0.17-0.79)	4
DICI-MT SCR-DOC	6.8 (6.8-6.8)	0.36 (0.36-0.36)	1

The range of NO_x emissions in each diesel vehicle group implied significant variation in the effectiveness of the same control technology (Table 5). Diesels using LNT only, regardless of number of turbochargers, returned median trip-level NO_x emissions of 0.41-0.43 g/km. Median trip-level emissions for diesels not using LNT were 0.25-0.36 g/km. At the extremes, the lowest and highest median emissions were 0.25 g/km and 0.64 g/km: the lower bound corresponded to a diesel with a single turbo and LNT; and the upper bound to a diesel with single turbo, LNT and DOC.

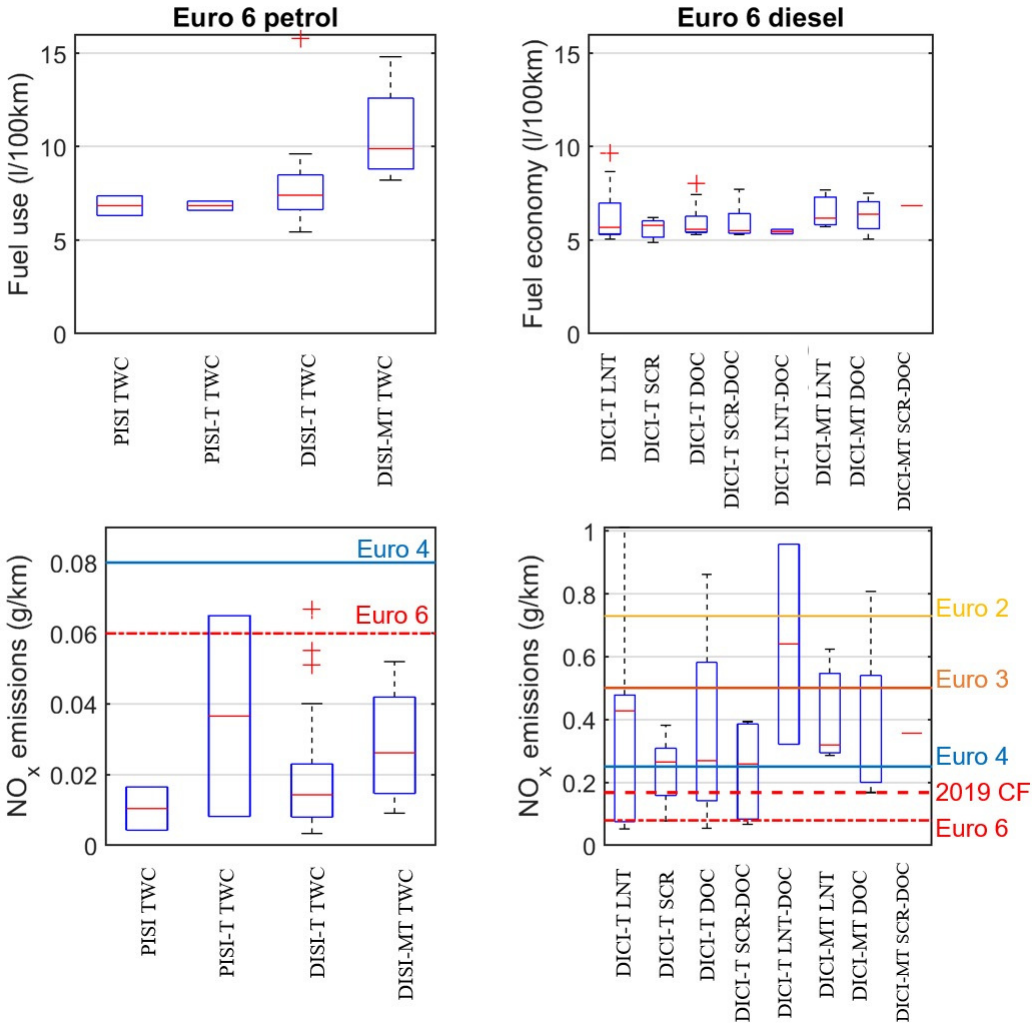

Figure 3: Boxplots of fuel economy (l/100 km) and NO_x emissions (g/km) for Euro 6 petrol (left column) and Euro 6 diesel vehicles (right column). Vehicle classification follows the definitions used in Table 1. Horizontal lines indicate the NO_x limits at various Euro standards.

3.2. Emissions factors by vehicle group

The vehicles used for model training and validation cover a broad range of engine performance (peak torque and power) and mass. Figure 4 illustrates the distribution of fuel economy and NO_x emissions based on engine performance and mass for training (orange circles) and test (blue crosses) vehicles across all groups. Fuel economy decreased (increasing values) with increasing vehicle mass and engine performance. Similarly, NO_x emissions fell (decreasing values) slightly with vehicle mass, but more prominently with engine performance. The training and validation vehicle data are mixed, with vehicles at the extremes of power, torque and mass used for training. This minimises the need for the QR models to extrapolate when estimating fuel use and NO_x emissions.

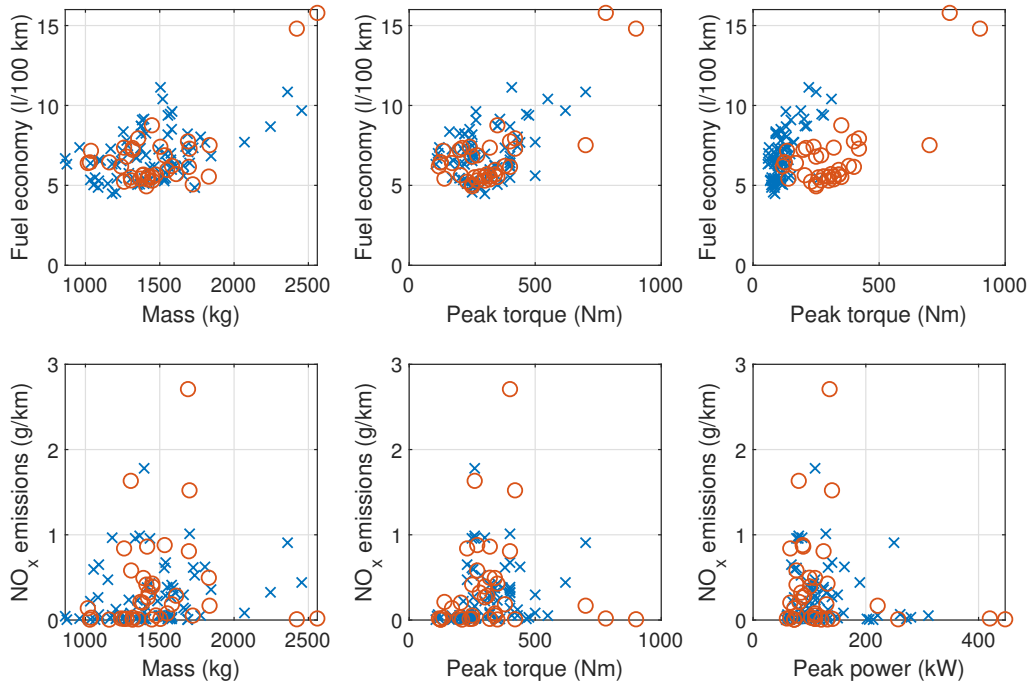

Figure 4: Distribution of fuel economy and NO_x emissions by engine performance (peak torque and peak power) and vehicle mass for training (orange circles) and test (blue crosses) vehicles across all groups.

For each vehicle group, the PEMS data from the test vehicles on the EA driving cycle is illustrated using orange, the validation set in blue, training data (based on simulations of the test vehicles) across 20 driving cycles in yellow and per second simulation of test vehicles using engine maps in purple. Figures B.8-B.25 illustrate the variation of fuel economy and NO_x emissions with each of the predictors across the three vehicle groups.

3.2.1. DISI with TWC

Seven vehicles were used for training and 23 for validation. Figure 5 gives the observed (purple) and predicted (green) fuel economy and NO_x emissions for the test vehicles (orange) and validation set (blue). The error bars indicate the 95% PI for each of the datasets from the QR model. The data is ordered from smallest PI to largest. Green circles exist for those vehicles where the QR model predicted fuel economy or NO_x to within 5% of observed. In this case, 20 vehicles lay within the 95% PI (four to within 5% of observed values, green circles) and three fell outside (red circles). For this latter group, values ranged from 1.2 l/100 km to 0.54 l/100 km below the lower bound of the 95% PI. The 95% PI enclosed the observed NO_x emissions for nine vehicles, with 14 lying outside (red circles). For these vehicles, observed NO_x ranged from 0.0031 g/km lower to 0.05 g/km higher.

Figure 5c and d compare the ability of COPERT and the QR model to predict fuel economy and NO_x emissions. The median predictive error of the QR model at 19% (0.5-71%) was better than that of COPERT at 23% (5-44%). The error in predicting NO_x emissions halved from 111% (8.7-920%) for COPERT to 53% (9.2-198%) for the QR model.

3.2.2. DICI with SCR

Three DICI vehicles with SCR were used for training and nine for validation. The 95% PI of the QR model enclosed fuel economy for three of the nine vehicles. The predicted fuel economy of the remaining six vehicles lay from 1.4 l/100 km below to 1.7 l/100 km above the bounds of the 95% PI. The 95% PI of the QR model for NO_x emissions enclosed all observed values. The predictive error for fuel economy using COPERT was 12% (0.7-34%) which was three times lower than the QR model at 34% (14-54%). The advantage of the QR model was more clear in predicting trip-level NO_x emissions with a median error of 49% (13-174%) which was half that of COPERT at 87% (37-705%).

3.2.3. DICI with LNT

There were 12 DICI vehicles with LNT in the training group and 20 for validation. The 95% PI of the QR model enclosed the fuel economy of 19 vehicles, four of them to within 5% of observed. One vehicle's fuel economy lay 1.6 l/100 km below the lower bound of the 95% PI. Likewise, the 95% PI of the QR model enclosed 19 of 20 NO_x observations, with one of them predicted to within 5% observed. One vehicle's NO_x emissions was 0.022 g/km below the lower bound of the 95% PI. Overall, predictive error of the QR model was 19% (1.5-48%) for fuel economy and 50% (2-728%) for NO_x emissions. COPERT was better at predicting fuel economy (median 14%, 95% PI = 0.32-31%), but worse for NO_x emissions (median 64%, 95% PI = 12-899%) as shown in Figure 7c and d. The results for the three vehicle groups are summarised in Table 6.

The large predictive error of 34% for the fuel economy QR model for DICI vehicles with SCR is due

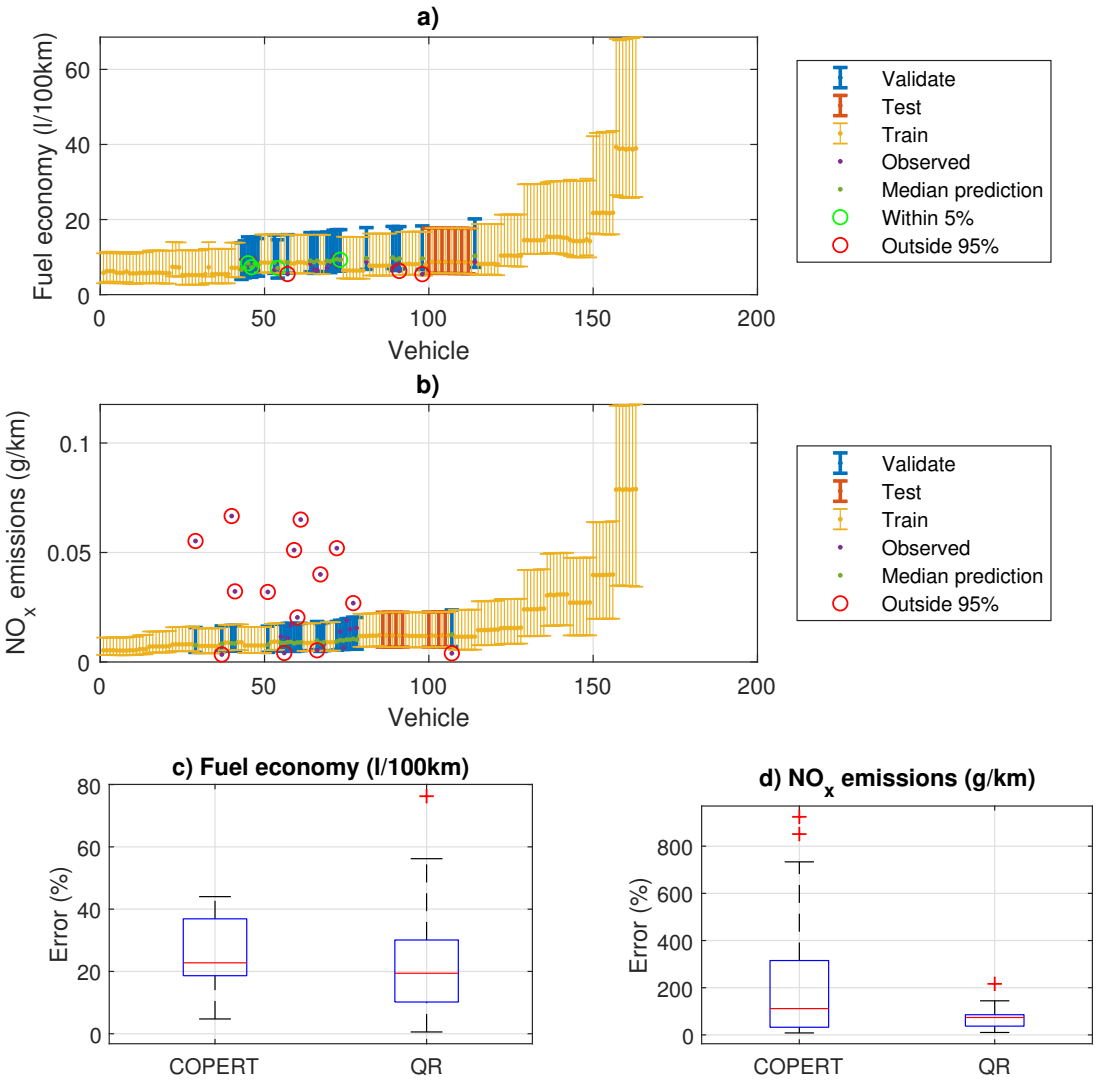

Figure 5: 95% prediction intervals for fuel economy (a) and NO_x emissions (b) of the test data (red) and validation data (blue) based on QR models trained on the training data (yellow) for DISI vehicles with TWC. Green circles indicate predictions (green dots) within 5% of observed (black dots). Red circles illustrate observations which fall outside of the 95% prediction interval. Boxplots comparing predictive accuracy using COPERT and QR over three percentiles to simulate the (c) fuel economy and (d) NO_x emissions of DISI vehicles. The lower and upper bounds of the boxes represent 2.5% and 97.5%.

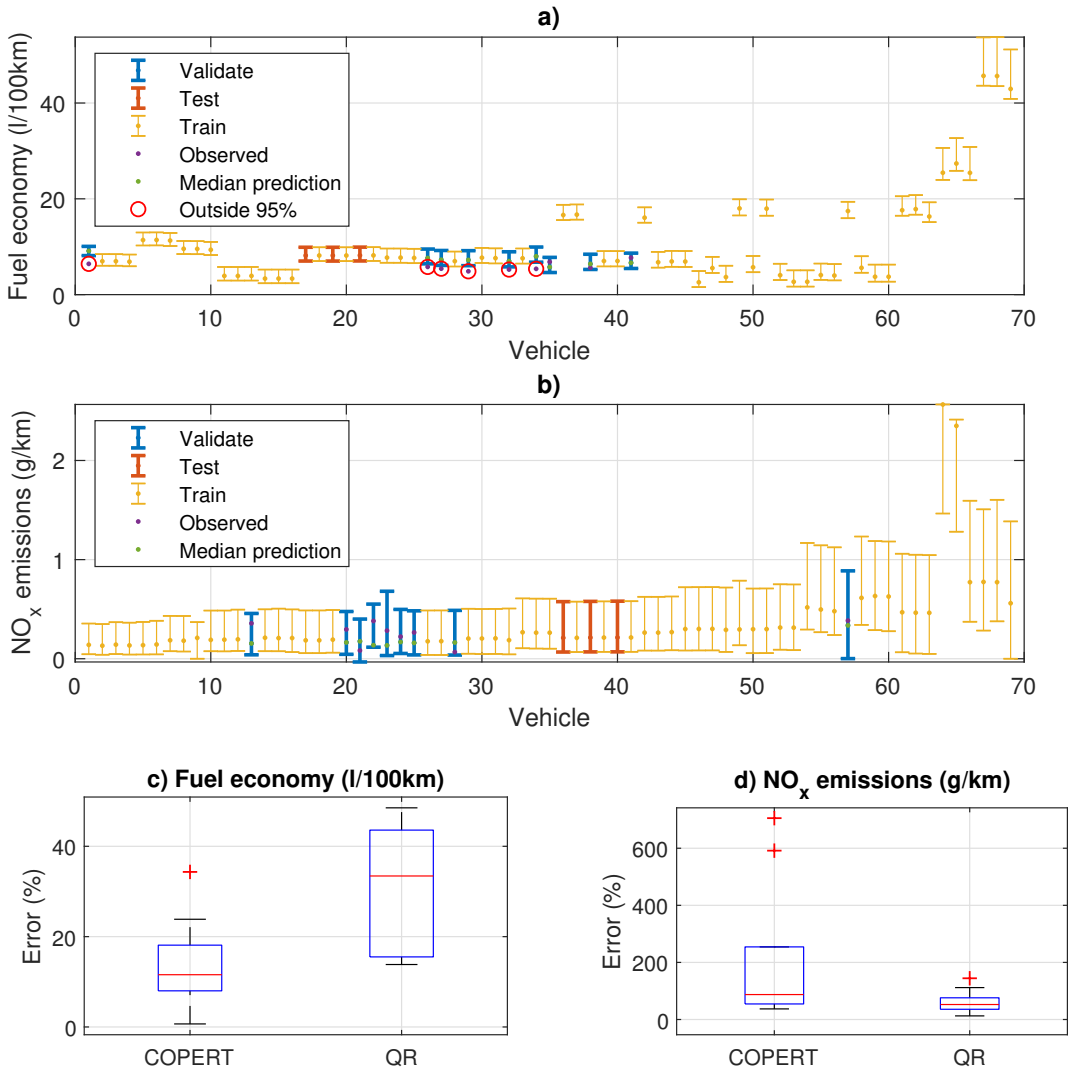

Figure 6: 95% prediction intervals for fuel economy (a) and NO_x emissions (b) of the test data (red) and validation data (blue) based on QR models trained on the training data (yellow) for DICI vehicles with SCR. Green circles indicate predictions (green dots) within 5% of observed (black dots). Red circles illustrate observations which fall outside of the 95% prediction interval. Boxplots comparing predictive accuracy using COPERT and the QR over three percentiles to simulate the (c) fuel economy and (d) NO_x emissions of DICI vehicles with SCR. The lower and upper bounds of the boxes represent 2.5% and 97.5%.

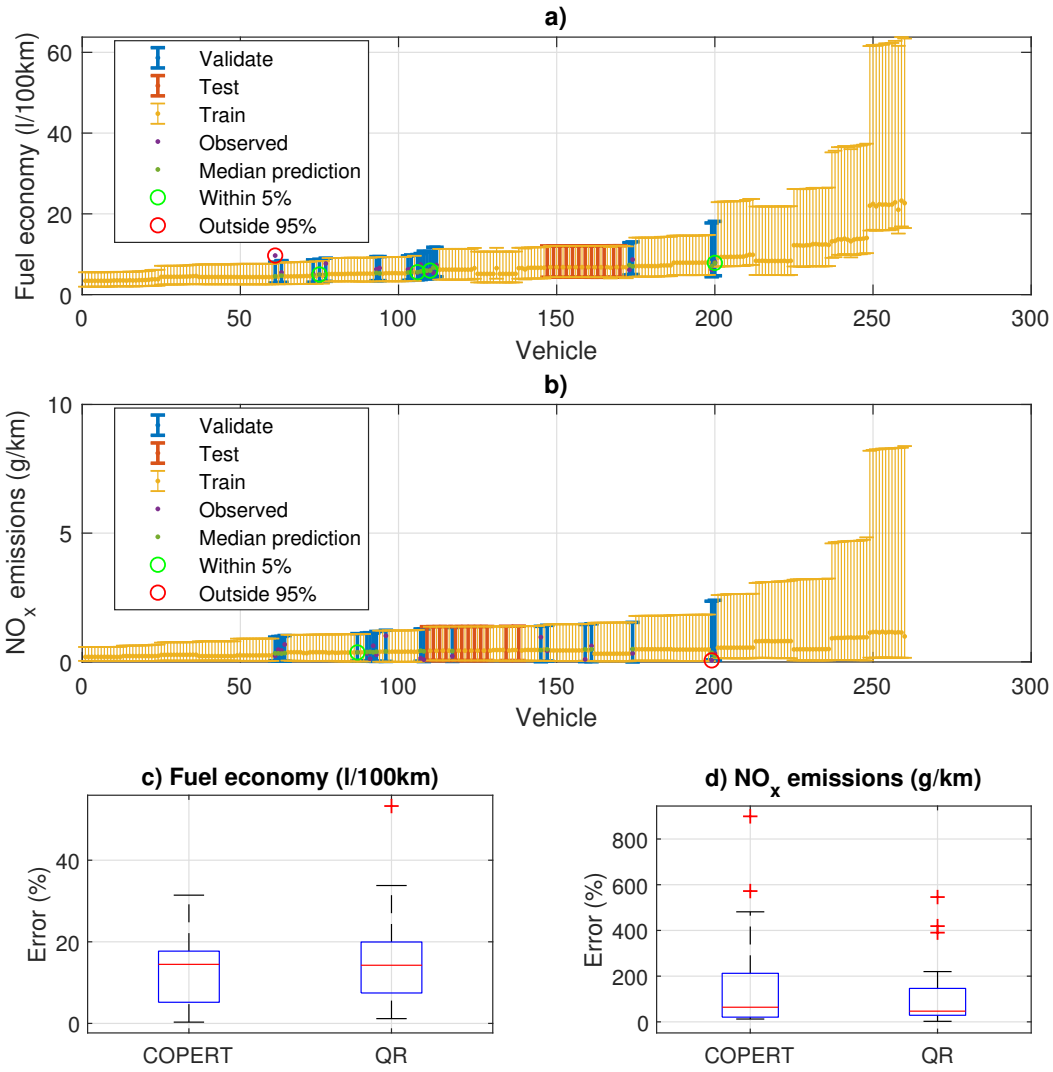

Figure 7: 95% prediction intervals for fuel economy (a) and NO_x emissions (b) of the test data (red) and validation data (blue) based on QR models trained on the training data (yellow) for DICI vehicles with LNT. Green circles indicate predictions (green dots) within 5% of observed (black dots). Red circles illustrate observations which fall outside of the 95% prediction interval. Boxplots comparing predictive accuracy using COPERT and the QR over three percentiles to simulate the (c) fuel economy and (d) NO_x emissions of DICI vehicles with LNT. The lower and upper bounds of the boxes represent 2.5% and 97.5%.

Table 6: Summary of factors in QR models using predictors x_i, $\frac{1}{x_i}$, $ln(x_i)$ and e_i^x with the lasso and elastic net, predictive accuracy with comparisons to the training set and COPERT for fuel economy and NO_x emissions

Fuel economy	DISI with TWC	DICI with SCR	DICI with LNT
5% accuracy (green circles)	4	0	4
Inside 95% PI	20	3	19
Outside 95% PI (red circles)	3	6	1
Total vehicles	23	9	20
Predictive accuracy - Training	19% (0.6-75%)	33% (14-49%)	14% (1.2-53%)
QR	19% (0.5-71%)	34% (14-54%)	19% (1.5-48%)
COPERT	23% (4.99-44%)	12% (0.7-34%)	14% (0.32-31%)
NO_x emissions			
5% accuracy (green circles)	0	0	1
Inside 95% PI	9	9	19
Outside 95% PI (red circles)	14	0	1
Total vehicles	23	9	20
Predictive accuracy - Training	74% (10.7-211%)	53% (13-144%)	47% (2-546%)
QR	53% (9.2-198%)	49% (13-174%)	50% (2-728%)
COPERT	111% (8.7-919%)	87% (37-705%)	64% (12-899%)

to only three training vehicles and nine test vehicles. In contrast, QR models for DISI vehicles with TWC and DICI vehicles with LNT used seven and 12 training vehicle respectively and returned similar predictive error of 19%. Notably, NO_x predictive error for the three vehicle groups was similar at 49-53%. This may be due the ability of exhaust treatment technologies to decouple engine out from tailpipe emissions, compressing the range of emissions within each vehicle class. However, fuel economy remains dependent on the characteristics of the vehicle and the way in which the are driven. Therefore, a broader set of training vehicles may be required to capture fuel economy more accurately.

3.3. Role of driving, vehicle and ambient characteristics in QR models

Employing the lasso and elastic net reduced the number of predictors in the QR models across the vehicle groups: the most sparse QR model with lasso used two variables; with up to nine added under the elastic net. The models for fuel economy and NO_x emissions depended on how the vehicle was driven and did not incorporate predictors of engine characteristics or the environmental conditions (Table 7). Across all groups and quantiles, QR models of fuel economy and NO_x emissions comprised four common predictors: number of stops per km, the KI of the driving and the inverse of RPSS and RPSC which all capture aspects of the dynamics of driving [15]. Additionally, the QR models of fuel economy for all vehicle groups used the exponential of median velocity and the inverse of each of median velocity, running velocity and aerodynamic velocity. The closed form equations for fuel economy are given in the following equations where coefficients are presented in the top to bottom order of the 2.5^{th}, 50^{th} and 97.5^{th} percentiles.

$$FE_{DISI} = \begin{cases} -1.384 \\ -0.886 \\ -0.316 \end{cases} \cdot stops + \begin{cases} 2.52 \\ 1.904 \\ 1.197 \end{cases} \cdot KI + \begin{cases} 7.152 \\ 4.988 \\ -18.655 \end{cases} \cdot \frac{1}{v_{run}} + \begin{cases} 36.449 \\ 39.815 \\ 59.345 \end{cases} \cdot \frac{1}{v_{median}} + \begin{cases} 424.829 \\ 435.09 \\ 626.793 \end{cases} \cdot \frac{1}{RPSS} + \begin{cases} 519.191 \\ 798.318 \\ 512.358 \end{cases} \cdot \frac{1}{RPSC}$$
$$+ \begin{cases} -525.781 \\ -554.602 \\ -597.919 \end{cases} \cdot \frac{1}{v_{aero}} + \begin{cases} 1.193 \\ 2.097 \\ 2.342 \end{cases} \cdot ln(RPSS) + \begin{cases} -71.296 \\ -72.831 \\ -90.966 \end{cases} \cdot e^{v_{median}} \quad (5)$$

$$FE_{DICI-SCR} = \begin{cases} -0.316 \\ 0.078 \\ 0.077 \end{cases} \cdot stops + \begin{cases} 6.588 \\ 6.593 \\ 7.58 \end{cases} \cdot KI + \begin{cases} -13.811 \\ -13.141 \\ -13.072 \end{cases} \cdot \frac{1}{v_{run}} + \begin{cases} 31.717 \\ 32.596 \\ 31.537 \end{cases} \cdot \frac{1}{v_{median}} + \begin{cases} 708.568 \\ 735.679 \\ 747.248 \end{cases} \cdot \frac{1}{RPSS} + \begin{cases} -504.452 \\ -528.815 \\ -482.179 \end{cases} \cdot \frac{1}{RPSC}$$
$$+ \begin{cases} -676.152 \\ -700.039 \\ -739.644 \end{cases} \cdot \frac{1}{v_{aero}} + \begin{cases} 15.209 \\ 15.194 \\ 14.642 \end{cases} \cdot ln(RPSS) + \begin{cases} -3215.345 \\ -3215.247 \\ -3213.232 \end{cases} \cdot ln(RPSC) + \begin{cases} 6415.732 \\ 6415.803 \\ 6413.257 \end{cases} \cdot ln(v_{aero}) + \begin{cases} -41.483 \\ -41.618 \\ -35.09 \end{cases} \cdot e^{v_{median}} \quad (6)$$

$$FE_{DICI-LNT} = \begin{cases} 0.769 \\ 1.501 \\ 1.918 \end{cases} \cdot stops + \begin{cases} -0.773 \\ -0.638 \\ -0.196 \end{cases} \cdot KI + \begin{cases} -13.274 \\ -19.679 \\ -19.653 \end{cases} \cdot \frac{1}{v_{run}} + \begin{cases} 4.951 \\ 3.727 \\ 13.745 \end{cases} \cdot \frac{1}{v_{median}} + \begin{cases} 214.49 \\ 222.784 \\ 286.325 \end{cases} \cdot \frac{1}{RPSS} + \begin{cases} -405.645 \\ -827.622 \\ -551.882 \end{cases} \cdot \frac{1}{RPSC}$$
$$+ \begin{cases} -131.816 \\ -74.934 \\ -93.371 \end{cases} \cdot \frac{1}{v_{aero}} + \begin{cases} 8.945 \\ 4.895 \\ 4.219 \end{cases} \cdot e^{v_{median}} \quad (7)$$

The QR models for NO_x emissions used a similar number of predictors: two predictors with the lasso, increasing to 10 with the elastic net. Models for DISI vehicle used only the four common predictors described earlier, while both groups of DICI vehicles used the inverse of aerodynamic velocity. DICI vehicles with SCR incorporated median VSP and additional dynamic predictors, such as median jolt and the exponential of median jolt. The closed form equations for fuel economy and NO_x emissions are given in the following equations where coefficients are presented in the top to bottom order of the 2.5^{th}, 50^{th} and 97.5^{th} percentiles.

Table 7: Metrics and coefficients of QR model to predict fuel economy and NO_x emissions across all groups of vehicles.

	DISI with TWC			DICI with SCR			DICI with LNT		
Fuel economy (mpg)	2.5%	50%	97.5%	2.5%	50%	97.5%	2.5%	50%	97.5%
Stops per km	-1.384	-0.886	-0.316	0.078	0.074	0.077	0.769	1.501	1.918
KI	2.52	1.904	1.197	6.588	6.593	7.58	-0.773	-0.638	-0.196
$\frac{1}{v_{run}}$	7.152	4.988	-18.655	-13.811	-13.141	-13.072	-13.274	-19.679	-19.653
$\frac{1}{v}$	36.449	39.815	59.345	31.717	32.596	31.537	4.951	3.727	13.745
$\frac{1}{RPSS}$	424.829	435.09	626.793	708.568	735.679	747.248	214.49	222.784	286.325
$\frac{1}{RPSC}$	519.191	798.318	512.358	-504.452	-528.815	-482.179	-405.645	-827.622	-551.882
$\frac{1}{v_{aero}}$	-525.781	-554.602	-597.919	-676.152	-700.039	-739.644	-131.816	-74.934	-93.371
ln(RPSS)	1.193	2.097	2.342	15.209	15.194	14.642	0	0	0
ln(RPSC)	0	0	0	-3215.345	-3215.247	-3213.232	0	0	0
ln(v_{aero})	0	0	0	6415.732	6415.803	6413.257	0	0	0
e^{v}	-71.296	-72.831	-90.966	-41.483	-41.618	-35.09	8.945	4.895	4.219
NO_x emissions (g/km)	2.5%	50%	97.5%	2.5%	50%	97.5%	2.5%	50%	97.5%
Stops per km	0.00144	0.00221	0.00234	0.05003	0.02644	0.0294	0.0617	0.01021	-0.09763
KI	0.00143	0.00098	0.00108	0.03758	0.09347	0.06933	-0.06433	0.23283	0.52221
Median Jolt	0	0	0	1.49858	-0.82133	1.18863	0	0	0
$\frac{1}{v_{run}}$	0	0	0	0	0	0	0.25674	0.17323	0.85157
$\frac{1}{v}$	0	0	0	0.33738	0.26747	0.57349	0	0	0
$\frac{1}{VSP}$	0	0	0	0.03833	0.05713	0.0306	0	0	0
$\frac{1}{RPSS}$	0.11577	0.16035	0.35067	-14.90976	-12.87782	-12.86008	-16.39374	33.47052	88.10547
$\frac{1}{RPSC}$	-0.78959	-0.11498	-0.33133	-62.60104	-69.06755	-83.59491	-2.72993	-108.2636	-32.50858
$\frac{1}{v_{aero}}$	0	0	0	21.40023	23.53968	29.91614	17.55356	-24.9662	-71.72115
ln(Median VSP)	0	0	0	0.02438	0.03671	0.023	0	0	0
$e^{Jolt_{iqr}}$	0	0	0	-0.16946	-0.23473	-0.17261	0	0	0

$$EF_{DISI} = \begin{cases} 0.00144 \\ 0.00221 \\ 0.00234 \end{cases} \cdot stops + \begin{cases} 0.00143 \\ 0.00098 \\ 0.00108 \end{cases} \cdot KI + \begin{cases} 0.11577 \\ 0.16035 \\ 0.35067 \end{cases} \cdot \frac{1}{RPSS} + \begin{cases} -0.78959 \\ -0.11498 \\ -0.33133 \end{cases} \cdot \frac{1}{RPSC} \tag{8}$$

$$EF_{DICI-SCR} = \begin{cases} 0.05003 \\ 0.02644 \\ 0.0294 \end{cases} \cdot stops + \begin{cases} 0.03758 \\ 0.09347 \\ 0.0.06933 \end{cases} \cdot KI + \begin{cases} 1.49858 \\ -0.82133 \\ 1.18863 \end{cases} \cdot jolt_{median} + \begin{cases} 0.33738 \\ 0.26747 \\ 0.57349 \end{cases} \cdot \frac{1}{v_{median}}$$

$$+ \begin{cases} 0.03833 \\ 0.05713 \\ 0.0306 \end{cases} \cdot \frac{1}{VSP_{median}} + \begin{cases} -14.90976 \\ -12.87782 \\ -12.86008 \end{cases} \frac{1}{RPSS} + \begin{cases} -62.60104 \\ -69.06755 \\ -83.59491 \end{cases} \cdot \frac{1}{RPSC} + \begin{cases} 21.40023 \\ 23.53968 \\ 29.91614 \end{cases} \cdot \frac{1}{v_{aero}} + \begin{cases} 0.02438 \\ 0.03671 \\ 0.023 \end{cases} \cdot ln(VSP_{median}) + \begin{cases} -0.16946 \\ -0.23473 \\ -0.17261 \end{cases} \cdot e^{Jolt_{median}} \tag{9}$$

$$EF_{DICI-LNT} = \begin{cases} 0.0617 \\ 0.01021 \\ -0.09763 \end{cases} \cdot stops + \begin{cases} -0.06433 \\ 0.23283 \\ 0.52221 \end{cases} \cdot KI + \begin{cases} 0.25674 \\ 0.17323 \\ 0.85157 \end{cases} \cdot \frac{1}{v_{run}} + \begin{cases} -16.39374 \\ 33.47052 \\ 88.10547 \end{cases} \cdot \frac{1}{RPSS} + \begin{cases} -2.72993 \\ -108.2636 \\ -32.50858 \end{cases} \cdot \frac{1}{RPSC} + \begin{cases} 17.55356 \\ -24.9662 \\ -71.72115 \end{cases} \cdot \frac{1}{v_{aero}} \tag{10}$$

3.4. QR model sensitivity

The lasso and elastic net penalties were designed to reduce the full set of predictors to those with the greatest influence. The sensitivity of the QR models to the number of variables was determined in two ways: first, using the lasso only to exclude correlated predictors from the final QR model; and second, using the smallest mean sum of errors under lasso and elastic net to return more full QR models.

Using the lasso only returned QR models which used up to two predictors for fuel economy and three predictors for NO_x emissions. The QR models predicted the fuel economy of ten DISI vehicles to within 5% of observed compared to four when the elastic net was considered. The NO_x emissions of two DICI vehicles with LNT were predicted to within 5% of observed with the lasso only, compared with one using the elastic net. Predictions to 5% accuracy were equal, with and without the elastic net, for fuel economy and NO_x emissions across the other cases. In general, removing correlated variables associated with the elastic net reduced the median predictive error up to 2.4 times across fuel use and NO_x emissions. The error in predicting fuel use of DICI vehicles with LNT was similar with and without the elastic net at 14.2-14.4%, while the error in predicting fuel use of DICI vehicles using SCR with elastic net was 2.8 times lower (12%) than with the lasso only (32%). The main advantage of incorporating correlated variables via the elastic net was the QR models returned narrower 95% PI than with the lasso only in all but one case (fuel economy for DISI vehicles): the smallest improvement in range was from 9.9% for NO_x emissions from DISI vehicles (9.2-198% with elastic net compared with 7.1-206% without) to 137% for NO_x emissions for DICI vehicles with LNT (1.6-728% with elastic net compared with 4.2-867% without elastic net). Including the elastic net for DICI vehicles with SCR reduced the PI range by 2.6 times for fuel economy, from 10-115% to 14-54%. The narrower PI implied the QR model was capturing real behaviour more accurately.

In the second analysis, QR models for fuel economy and NO_x emissions used up to 110 predictors and 46 predictors, respectively. The results in Table 9 show the QR models were less accurate in predicting fuel economy and NO_x emissions compared to the base case: the median prediction error was higher; the 95% PI were wider; and the QR model predicted the outputs of fewer vehicles to within 5% of observed. Therefore, the approach used in this work trades broader model accuracy through narrower PI for small decreases in median predictive accuracy.

Table 8: Summary of factors in QR models using predictors x_i, $\frac{1}{x_i}$, $ln(x_i)$ and e_i^x with the lasso only, predictive accuracy with comparisons to the training set and COPERT for fuel economy and NO_x emissions.

Fuel economy	DISI with TWC	DICI with SCR	DICI with LNT
5% accuracy (green circles)	10	0	4
Inside 95% PI	23	6	19
Outside 95% PI (red circles)	0	3	1
Total vehicles	23	9	20
Predictive accuracy - Training	9% (0.3-42%)	30% (10-115%)	23% (0.5-75%)
QR	14% (0.5-46%)	32% (10-115%)	14% (0.8-69%)
COPERT	23% (4.99-44%)	12% (0.7-34%)	14% (0.32-31%)
NO_x emissions			
5% accuracy (green circles)	0	0	2
Inside 95% PI	9	8	19
Outside 95% PI (red circles)	14	1	1
Total vehicles	23	9	20
Predictive accuracy - Training	73% (13.1-219%)	35% (8-202%)	51% (4-1003%)
QR	54% (7.1-206%)	37% (8-209%)	57% (4-867%)
COPERT	111% (8.7-919%)	87% (37-705%)	64% (12-899%)

Table 9: Summary of factors in QR models using the expanded predictor set of x_i, $\frac{1}{x_i}$, $ln(x_i)$ and e_i^x, x^2 and $\frac{1}{x^2}$ which returned smallest mean squared error with the lasso and elastic net, predictive accuracy with comparisons to the training set, COPERT and simulations for fuel economy and NO_x emissions

Fuel economy	DISI with TWC	DICI with SCR	DICI with LNT
5% accuracy (green circles)	0	0	0
Inside 95% PI	0	0	1
Outside 95% PI (red circles)	23	9	19
Total vehicles	23	9	20
Predictive accuracy - Training	114171% (982-483605%)	12973% (2999-18393%)	3211% (37-12011%)
QR	54475% (1.7-456751%)	10708% (56-18393%)	791% (4.6-11294%)
COPERT	23% (5-44%)	12% (0.7-34%)	14% (0.32-31%)
NO_x emissions			
5% accuracy (green circles)	0	0	1
Inside 95% PI	0	1	13
Outside 95% PI (red circles)	23	8	7
Total vehicles	23	9	20
Predictive accuracy - Training	3154% (5.2-1978431%)	1283% (36-128509%)	101% (4-3720%)
QR	539% (5.9-1627831%)	421% (24-128509%)	55% (4-2780%)
COPERT	111% (8.7-919%)	87% (37-705%)	64% (12-899%)

4. Benefits to the approach and future improvements

There has been considerable research effort into both identifying and quantifying the increasing discrepancy between type approval and real-world fuel economy and emissions. However, knowing the size of this mismatch does not give us the tools to predict fuel economy and NO_x emissions accurately.

In this work, Euro 6 vehicles were grouped by fuel-air system and exhaust gas after-treatment technology. A QR model for each of fuel economy and NO_x emissions by vehicle group was trained using a subset of driving cycle, vehicle and ambient predictors. The performance of the QR was assessed using a 95% PI around the observed value from a validation PEMS dataset. Metrics representing the dynamics of the driving cycles (stops per km, KI, RPSS and RPSC) contributed most to the QR models of fuel economy and NO_x emissions, rather than engine characteristics or ambient conditions.

Our previous work on engine mapping is aimed at vehicle level accuracy. This work complements that research by providing a bottom-up, transparent method for deriving emissions factors. However, there is a trade-off between the effort in collecting all available data from a vehicle and predicting the fuel use and NO_x emissions from a class of vehicles. Emissions factors which can be applied to traffic flows and composition along a road link should be derivable from readily observable data, such as driving cycles and ambient conditions. Some vehicle specific data, such as air-fuel ratio or catalyst temperature would aid the prediction of fuel use and emissions. However, they cannot be collected remotely at the fleet level. The boxes in Figure 3 illustrate the broad range of fuel use and NO_x emissions both between and within the groups of vehicles used in this work. Our approach internalises the analytical difficulties of deriving models over such ranges by focusing on the PI which enclose the observed data at the expense of some median prediction accuracy.

QR models returned accuracy comparable with COPERT for fuel economy across the vehicle groups. The exception was for DICI vehicles with SCR for which the median COPERT prediction error of 12% was almost three times lower than the QR model at 34%. This relatively large predictive error may be attributed to only three training vehicles available. The advantages of the approach manifest in improved predictions of NO_x emissions, with median error falling by 28% for DICI vehicles with LNT and by half for both DISI vehicles and DICI vehicles with SCR. Moreover, all observed values for DICI vehicles with SCR and 19 of 20 for DICI with LNT fell within the QR model's 95% PI. This is encouraging as modern exhaust after-treatment technologies decouple effectively engine out from tailpipe emissions, making it more difficult to use physics-based, vehicle dynamic approaches to estimate emissions accurately. Using the lasso with elastic net to produce a reduced predictor set returned QR models with optimum predictive accuracy.

The approach described in this work has a number of advantages. First, it uses internally-consistent powertrain models of vehicles in service which incorporate explicitly the range of technologies deployed. Repeating this analysis on Euro 5 through to RDE-compliant Euro 6 vehicles would offer insight into how

fuel economy and NO_x emissions have changed with engine and exhaust after-treatment technology. Second, the method for developing the QR models allows new training cycles, training vehicles, metrics and modelling approaches to be added over time to maintain and improve the QR predictive accuracy. This flexibility and future proofing is important because the width of the 95% PI and the number of vehicles falling outside of it implies important predictors are missing from the models.

There are areas where this work can be expanded. Namely, the vehicles were driven conservatively (gears shifted up at lower engine speeds) during the PEMS test. Consequently, the full torque-speed range of engine operation was not available to create the engine maps. Additionally, the gear shift regime observed on the PEMS test was maintained during the training cycle simulations. Therefore, the fuel economy and NO_x emissions across the training cycles implicitly assume the same driver (and driving approach) as on the original PEMS test. Future PEMS testing could be longer in duration and conducted under varied ambient and driving behaviour conditions to characterise the vehicles more fully. For example, more testing of aggressive driving (gears shifted up at higher engine speeds) under different ambient conditions might return fuel economy and NO_x emissions with stronger dependence on engine characteristics and ambient conditions. Finally, expanding the PEMS regime to include engine out emissions would isolate the effect of exhaust after-treatment technologies.

5. Acknowledgements

The authors acknowledge the UK EPSRC funding provided for this work under the Centre for Sustainable Road Freight Transport (EP/K00915X/1) and the Energy Efficient Cities Initiative (EP/F034350/1). The authors acknowledge the assistance of Wesley Blank in gathering vehicle specification data.

Additional data related to this publication is available at the University of Cambridge data repository (tbc).

6. References

[1] E. Commission, COMMISSION REGULATION (EU) 2016/ 427 - of 10 March 2016 - amending Regulation (EC) No 692 / 2008 as regards emissions from light passenger and commercial vehicles (Euro 6).

[2] EC, Setting emission performance standards for new passenger cars as part of the Community's integrated approach to reduce CO2 emissions from light-duty vehicles, no. 443/2009, Official Journal of the European Union, 2009.

[3] EEA, Fuel efficiency improvements of new cars in Europe slowed in 2016, Tech. rep., European Environment Agency (2017).
URL https://www.eea.europa.eu/highlights/fuel-efficiency-improvements-of-new

[4] U. Tietge, S. Díaz, P. Mock, A. Bandivadekar, J. Dornoff, N. Ligterink, From laboratory to road: A 2018 update of official and "real-world" fuel consumption and CO_2 values for passenger cars in Europe, 2019.

[5] U. Tietge, S. Díaz, P. Mock, J. German, A. Bandivadekar, N. Ligterink, From laboratory to road: A 2016 update of official and "real-world" fuel consumption and CO_2 values for passenger cars in Europe, 2016.

[6] U. Tietge, P. Mock, J. German, A. Bandivadekar, N. Ligterink, From Laboratory to Road: A 2017 update of official and "real-world" fuel consumption and CO_2 values for passenger cars in Europe, 2017.

[7] ACEA, Economic and Market Report: EU Automotive Industry Quarter 4 2017, Tech. rep., European Automobile Manufacturers Association (2018).
URL http://www.acea.be/uploads/statistic{_}documents/Economic{_}and{_}Market{_}Report{_}Q4{_}2017.pdf

[8] EEA, No improvements on average CO2 emissions from new cars in 2017, 2018.
URL https://www.eea.europa.eu/highlights/no-improvements-on-average-co2/?utm{_}medium=email{&}utm{_}campaign=No%20improvements%20on%20average%20CO2%20emissions%20from%20new%20cars%20in%202017{&}utm{_}content=No%20improvements%20on%20average%20CO2%20emissions%20from%20n

[9] EC, Commission Regulation (EC) No 692/2008 of 18 July 2008 implementing and amending Regulation (EC) No 715/2007 of the European Parliament and of the Council on type-approval of motor vehicles with respect to emissions from light passenger and commercial veh, 2008.

[10] C. Baldino, U. Tietge, R. Muncrief, Y. Bernard, P. Mock, Road tested: Comparative overview of real-world versus type-approval NOx and CO2 emissions from diesel cars in Europe, 2017.

[11] B. Degraeuwe, M. Weiss, Does the New European Driving Cycle (NEDC) really fail to capture the NOx emissions of diesel cars in Europe?, Environmental Pollution 222 (2017) 234–241. doi:10.1016/J.ENVPOL.2016.12.050.
URL http://www.sciencedirect.com/science/article/pii/S0269749116327476

[12] M. Rexeis, S. Hausberger, J. Kühlwein, R. Luz, Update of Emission Factors for EURO 5 and EURO 6 vehicles for the HBEFA Version 3 . 2, University of Technology, Graz, Report Nr. I-31/2013 Rex-EM-Idoi:ReportNo.I-25/2013/RexEM-I2011/20679.

[13] S. Hausberger, Update of Emission Factors for EURO 4, EURO 5 and EURO 6 Diesel Passenger Cars for the HBEFA Version 3.3, Tech. rep. (2017).
URL http://www.hbefa.net/e/documents/HBEFA3-3{_}TUG{_}finalreport{_}01062016.pdf

[14] M. Pathak, P. R. Shukla, Co-benefits of low carbon passenger transport actions in Indian cities: Case study of Ahmedabad, Transportation Research Part D: Transport and Environment 44 (2016) 303–316. doi:10.1016/j.trd.2015.07.013.

[15] T. Barlow, S. Latham, I. McCrae, P. G. Boulter, A reference book of driving cycles for use in the measurement of road vehicle emissions, 2009.
URL https://trl.co.uk/access-publication?download{_}title=A+reference+book+of+driving+cycles+for+use+in+the+measurement+of+road+vehicle+emissions{&}download{_}url=https{%}3A{%}2F{%}2Ftrl.co.uk{%}2Fsites{%}2Fdefault{%}2Ffiles{%}2FPPR354{_}new.pdf

[16] J. Gallus, U. Kirchner, R. Vogt, T. Benter, Impact of driving style and road grade on gaseous exhaust emissions of passenger vehicles measured by a Portable Emission Measurement System (PEMS), Transportation Research Part D: Transport and Environment 52 (2017) 215–226. doi:10.1016/j.trd.2017.03.011.

[17] J. M. Luján, V. Bermúdez, V. Dolz, J. Monsalve-Serrano, An assessment of the real-world driving gaseous emissions from a Euro 6 light-duty diesel vehicle using a portable emissions measurement system (PEMS), Atmospheric Environment 174 (2018) 112–121. doi:10.1016/j.atmosenv.2017.11.056.
URL http://linkinghub.elsevier.com/retrieve/pii/S1352231017308178

[18] L. Ntziachristos, G. Mellios, D. Tsokolis, M. Keller, S. Hausberger, N. E. Ligterink, P. Dilara, In-use vs. type-approval fuel consumption of current passenger cars in Europe, Energy Policy 67 (2014) 403–411. doi:10.1016/J.ENPOL.2013.12.013.
URL http://www.sciencedirect.com/science/article/pii/S0301421513012573

[19] U. Tietge, P. Mock, V. Franco, N. Zacharof, From laboratory to road: Modeling the divergence between official and real-world fuel consumption and CO2 emission values in the German passenger car market for the years 2001-2014, Energy Policy 103 (2017) 212–222. doi:10.1016/j.enpol.2017.01.021.

URL http://www.sciencedirect.com/science/article/pii/S0301421517300320?via{%}3Dihub

[20] S. Kwon, Y. Park, J. Park, J. Kim, K. H. Choi, J. S. Cha, Characteristics of on-road NOx emissions from Euro 6 light-duty diesel vehicles using a portable emissions measurement system, Science of the Total Environmentdoi:10.1016/j.scitotenv.2016.10.101.

[21] L. Ntziachristos, G. Papadimitriou, N. Ligterink, S. Hausberger, Implications of diesel emissions control failures to emission factors and road transport NOx evolution, Atmospheric Environment 141 (2016) 542–551. doi:10.1016/J.ATMOSENV.2016.07.036.

URL http://www.sciencedirect.com/science/article/pii/S1352231016305568

[22] C.-L. Myung, W. Jang, S. Kwon, J. Ko, D. Jin, S. Park, Evaluation of the real-time de-NOx performance characteristics of a LNT-equipped Euro-6 diesel passenger car with various vehicle emissions certification cycles, Energy 132 (2017) 356–369. doi:10.1016/j.energy.2017.05.089.

URL http://www.sciencedirect.com/science/article/pii/S0360544217308472

[23] EPA, Population and Activity of On-road Vehicles in MOVES2014, 2016.
URL http://nepis.epa.gov/Exe/ZyPDF.cgi?Dockey=P100O7VJ.pdf

[24] G. O. Duarte, G. A. Gonçalves, T. L. Farias, Analysis of fuel consumption and pollutant emissions of regulated and alternative driving cycles based on real-world measurements, Transportation Research Part D: Transport and Environmentdoi:10.1016/j.trd.2016.02.009.

[25] L. Qu, M. Li, D. Chen, K. Lu, T. Jin, X. Xu, Multivariate analysis between driving condition and vehicle emission for light duty gasoline vehicles during rush hours, Atmospheric Environment 110 (2015) 103–110. doi:10.1016/j.atmosenv.2015.03.038.

[26] R. A. Rodríguez, E. A. Virguez, P. A. Rodríguez, E. Behrentz, Influence of driving patterns on vehicle emissions: A case study for Latin American cities, Transportation Research Part D: Transport and Environment 43 (2016) 192–206.
URL http://www.sciencedirect.com/science/article/pii/S1361920915002187{#}f0025

[27] K. M. Sentoff, L. Aultman-Hall, B. A. Holmén, Implications of driving style and road grade for accurate vehicle activity data and emissions estimates, Transportation Research Part D: Transport and Environment 35 (2015) 175–188. doi:10.1016/j.trd.2014.11.021.

URL http://linkinghub.elsevier.com/retrieve/pii/S1361920914001849

[28] EPA, Exhaust Emission Rates for Light-Duty On-road Vehicles in MOVES2014: Final Report, 2015.
URL http://nepis.epa.gov/Exe/ZyPDF.cgi?Dockey=P100NNVN.pdf

[29] T. Lee, J. Park, S. Kwon, J. Lee, J. Kim, Variability in operation-based NOx emission factors with different test routes, and its effects on the real-driving emissions of light diesel vehicles, Science of the Total Environment 461-462 (2013) 377–385. doi:10.1016/j.scitotenv.2013.05.015.

URL http://www.sciencedirect.com/science/article/pii/S0048969713005585?via{%}3Dihub

[30] R. Jaikumar, S. Shiva Nagendra, R. Sivanandan, Modeling of real time exhaust emissions of passenger cars under heterogeneous traffic conditions, Atmospheric Pollution Research 8 (1) (2017) 80–88. doi:10.1016/j.apr.2016.07.011.
URL http://www.sciencedirect.com/science/article/pii/S1309104216300691

[31] D. C. Carslaw, G. Rhys-Tyler, New insights from comprehensive on-road measurements of NOx, NO2 and NH3 from vehicle emission remote sensing in London, UK, Atmospheric Environment 81 (2013) 339–347. doi:10.1016/j.atmosenv.2013.09.026.

URL http://linkinghub.elsevier.com/retrieve/pii/S1352231013007140

[32] J. D. K. Bishop, M. E. J. Stettler, N. Molden, A. M. Boies, Engine maps of fuel use and emissions from transient driving cycles, Applied Energy 183 (2016) 202–217. doi:10.1016/j.apenergy.2016.08.175.

[33] L. F. Burgette, J. P. Reiter, M. L. Miranda, Exploratory Quantile Regression With Many Covariates, Epidemiology 22 (6)

(2011) 859–866. doi:10.1097/EDE.0b013e31822908b3.
URL http://content.wkhealth.com/linkback/openurl?sid=WKPTLP:landingpage{&}an=00001648-201111000-00016

[34] C. Guddat, U. Grouven, R. Bender, G. Skipka, A note on the graphical presentation of prediction intervals in random-effects meta-analyses., Systematic reviews 1 (2012) 34. doi:10.1186/2046-4053-1-34.
URL http://www.pubmedcentral.nih.gov/articlerender.fcgi?artid=3552946{&}tool=pmcentrez{&}rendertype=abstract

[35] L. Ntziachristos, Z. Samaras, EMEP/EEA air pollutant emission inventory guidebook 2016, 2017.
URL https://www.eea.europa.eu/publications/emep-eea-guidebook-2016/part-b-sectoral-guidance-chapters/1-energy/1-a-combustion/1-a-3-b-i/view

Appendix A. Engine Mapper improvements

Appendix A.1. Extract vehicle characteristics and engine maps

A modified version of the engine mapper approach[32] was employed in this paper. The modifications include a more robust gear ratio identification method, incorporation of RMS error for outliers of the fuel use and emissions time series and introduction of the interquartile range (IQR) to capture the distribution of fuel use and emissions in each area of the engine map.

A logistic curve ($Qpre$) was fit to the engine coolant time series. Hot running was considered to begin when engine coolant temperature stabilised which occurred when the first order difference of $Qpre$ became less than 0.01 for the first time:

$$t_{hot} = (Qpre_{i+1} - Qpre_i) < 0.01 \tag{A.1}$$

where i is the i^{th} value of the $Qpre$ logistic fit to the engine coolant time series. A binary variable, hot_ind, was set to 1 for instances where either this condition was not met or no engine coolant temperature was reported. The driving cycle representing hot running began at the first index with zero wheel speed after t_{hot}.

Appendix A.1.1. New gear ratios

Initially, the highest wheel speed was assumed to correspond to the highest engine speed [32]. However, this assumption is not robust to the range of driving behaviours observed in the population. Instead, this work uses the 5^{th} to the 95^{th} percentile of wheel speed v, denoted v_{5-95}, and corresponding engine speed to identify the top gear and bottom gear. The engine speed at top gear was the median of engine speeds around the maximum wheel speed (that is, v_{max}±1 m/s). This range ensured multiple data points existed in the region of v_{max} to return a median. The maximum of v_{5-95} (and the corresponding engine speed) accounted for situations where the highest engine speed did not correspond to the top gear. The minimum of v_{5-95} and corresponding engine speed were assigned to operation in first gear.

Appendix A.1.2. Incorporation of outliers

The original engine mapping work used the sum of absolute deviations (SAD) between simulated and observed values, recognising that RMS error prioritises outliers over values closer to the median [32]. In this work, a logical AND is applied to the SAD and RMS error values to incorporate outliers while not sacrificing the accuracy around the median. The logical AND was applied on a per second basis in two places: first, to determine the most likely vehicle configuration based on the deviation in engine speed between observed and simulated; and second, to determine the optimum bin for developing the engine map based on the deviation between observed and simulated fuel use and emissions.

Appendix A.1.3. Uncertainty in engine maps

Initially, engine maps were based on the mean value of each bin to determine that which reproduced best the observed values [32]. The challenge of developing engine maps of fuel use and emissions from on-the-go driving occurs because a distribution of values exists for a given engine torque-speed point, rather than a constant value which would be obtained from a steady-state test. The mean was used because its low breakdown threshold internalises outliers. The bin number corresponding to the smallest product of SAD and RMSE was chosen for the map.

Appendix B. Fuel economy and emissions simulation outputs

Figures B.8-B.25 illustrate the results of the simulations of training vehicles (orange circles) across the driving cycles (yellow dots). Validation vehicles are shown as blue crosses in each pane.

Appendix B.1. DISI with TWC

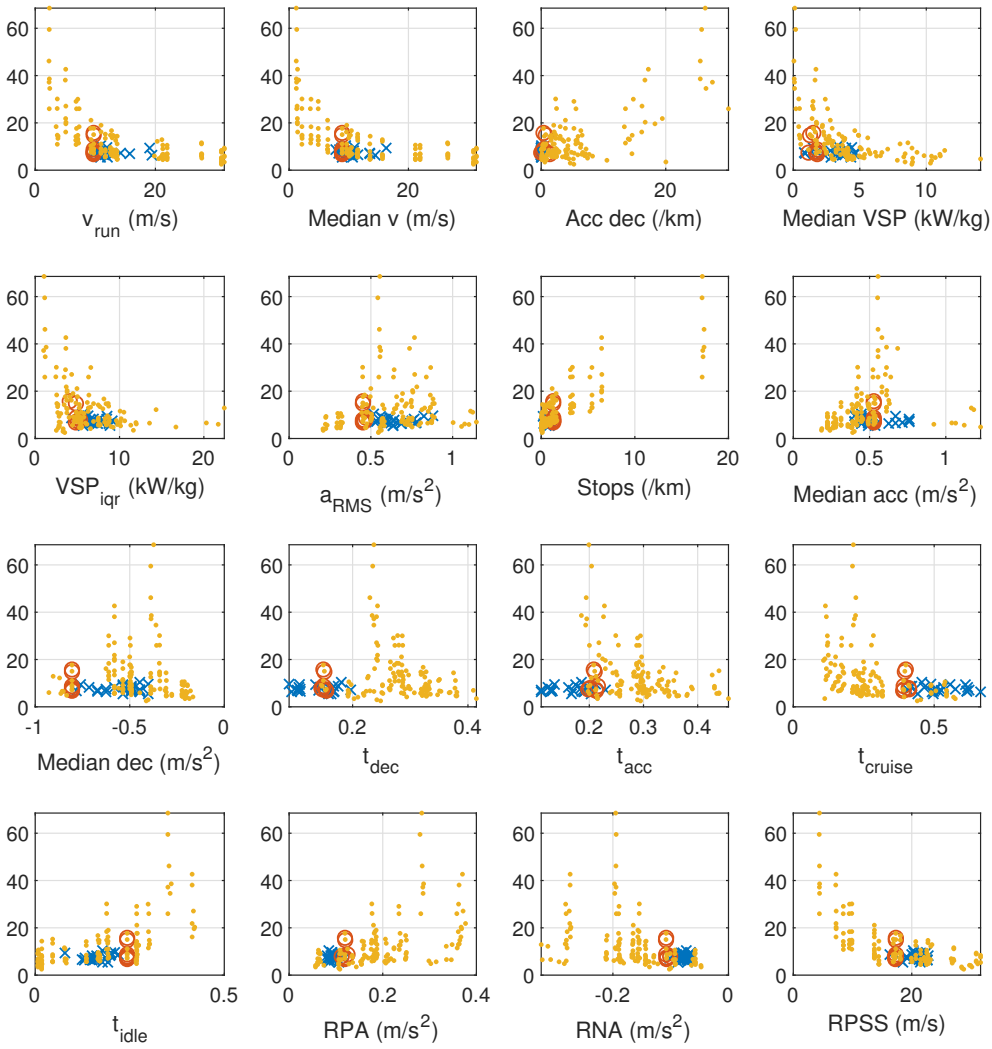

Figure B.8: Scatter plots of fuel economy (l/100 km) against QR predictors for simulated data (yellow dots), training vehicles on the EA PEMS cycle (orange circles) and validation vehicles (blue crosses).

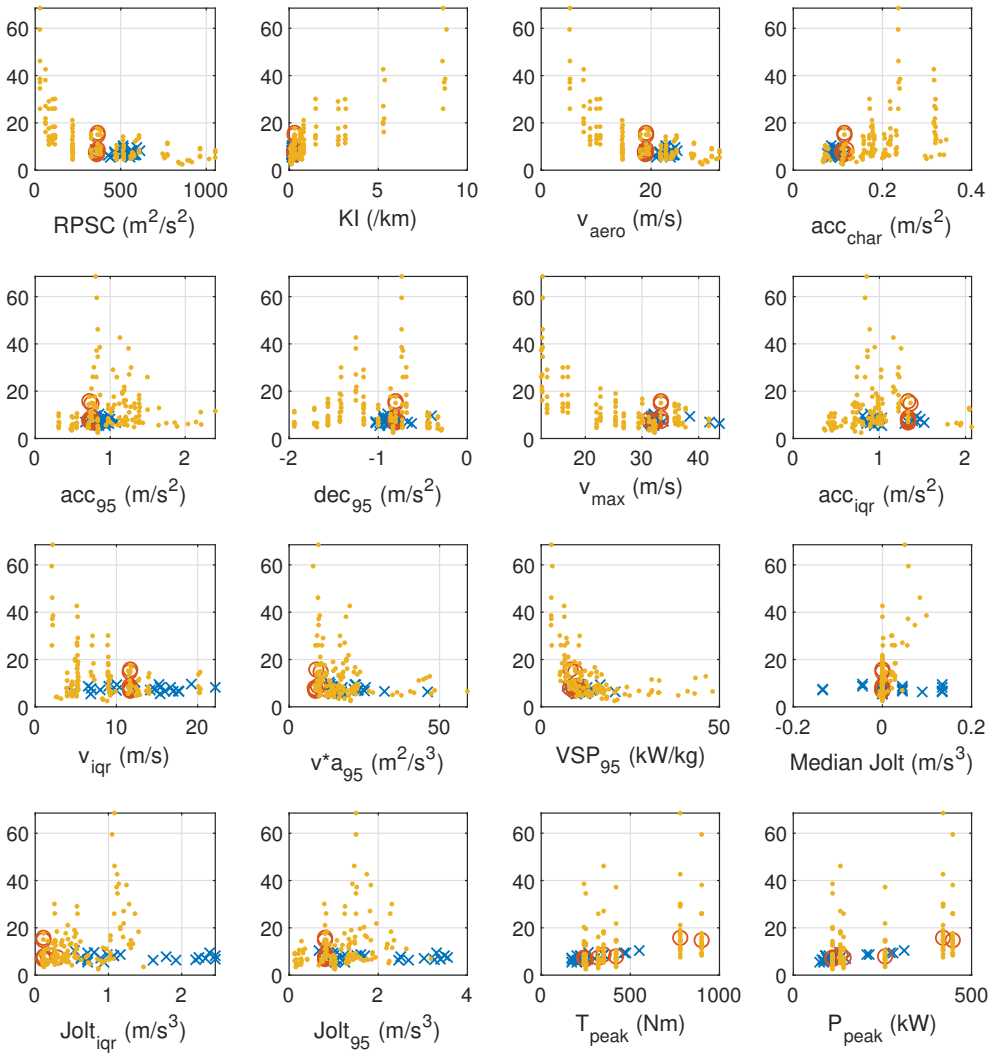

Figure B.9: Scatter plots of fuel economy (l/100 km) against QR predictors for simulated data (yellow dots), training vehicles on the EA PEMS cycle (orange circles) and validation vehicles (blue crosses).

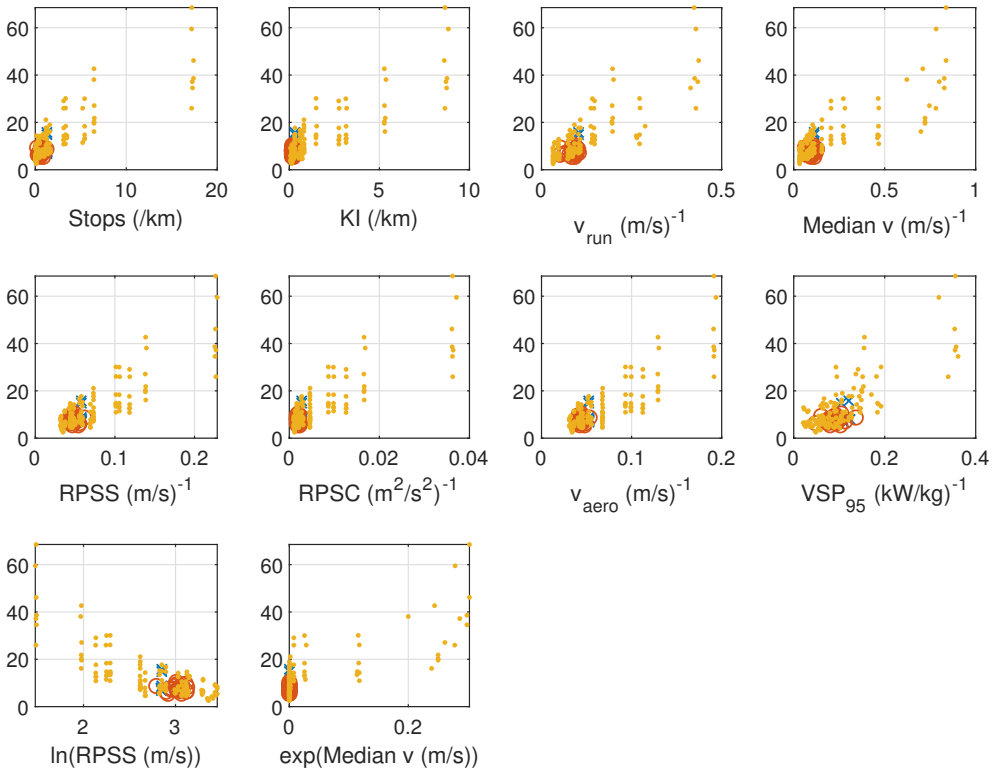

Figure B.10: Scatter plots of fuel economy (l/100 km) against QR predictors for simulated data (yellow dots), training vehicles on the EA PEMS cycle (orange circles) and validation vehicles (blue crosses).

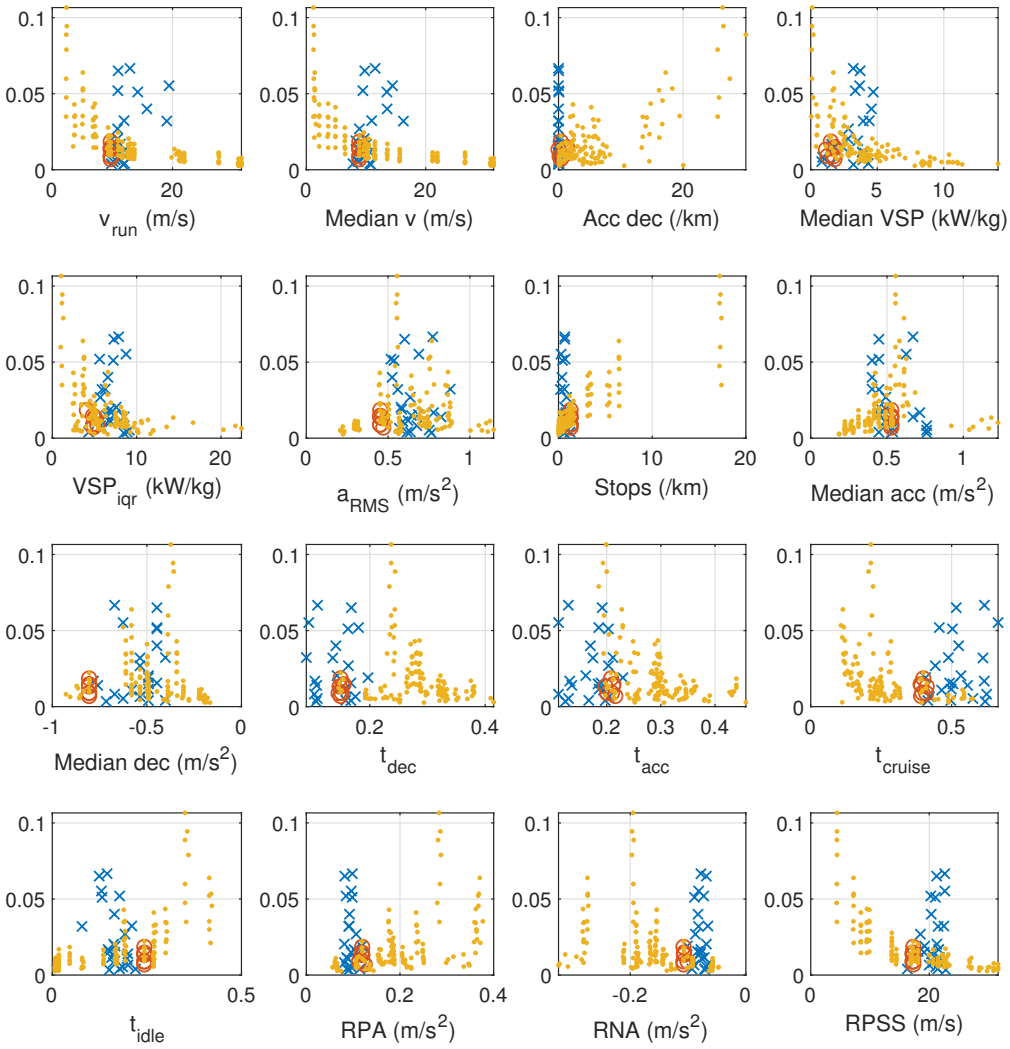

Figure B.11: Scatter plots of NO_x emissions (g/km) against QR predictors for simulated data (yellow dots), training vehicles on the EA PEMS cycle (orange circles) and validation vehicles (blue crosses).

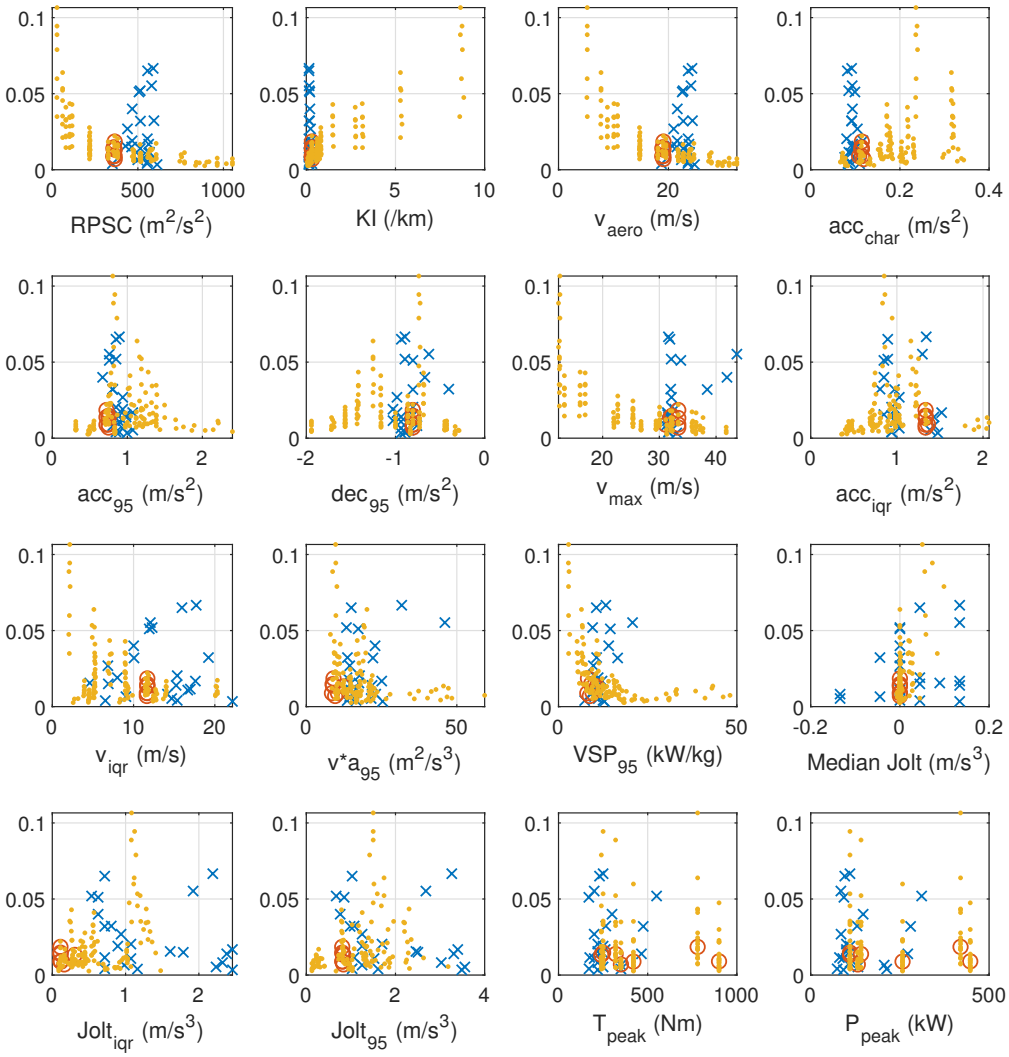

Figure B.12: Scatter plots of NO_x emissions (g/km) against QR predictors for simulated data (yellow dots), training vehicles on the EA PEMS cycle (orange circles) and validation vehicles (blue crosses).

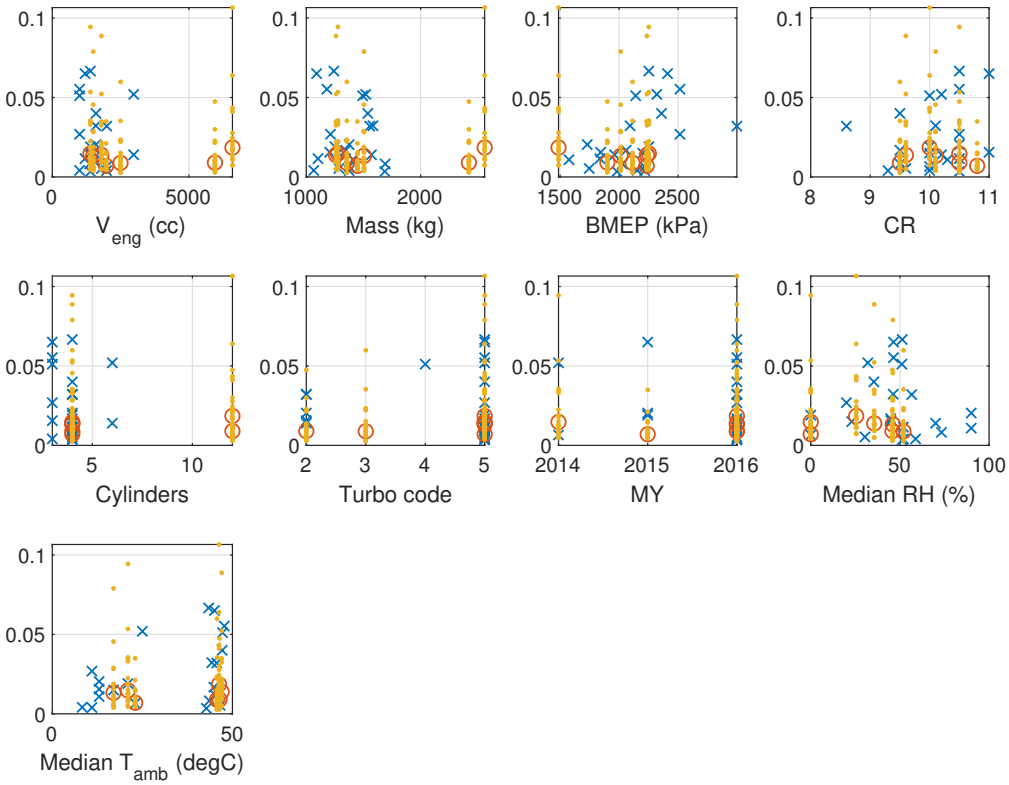

Figure B.13: Scatter plots of NO_x emissions (g/km) against QR predictors for simulated data (yellow dots), training vehicles on the EA PEMS cycle (orange circles) and validation vehicles (blue crosses).

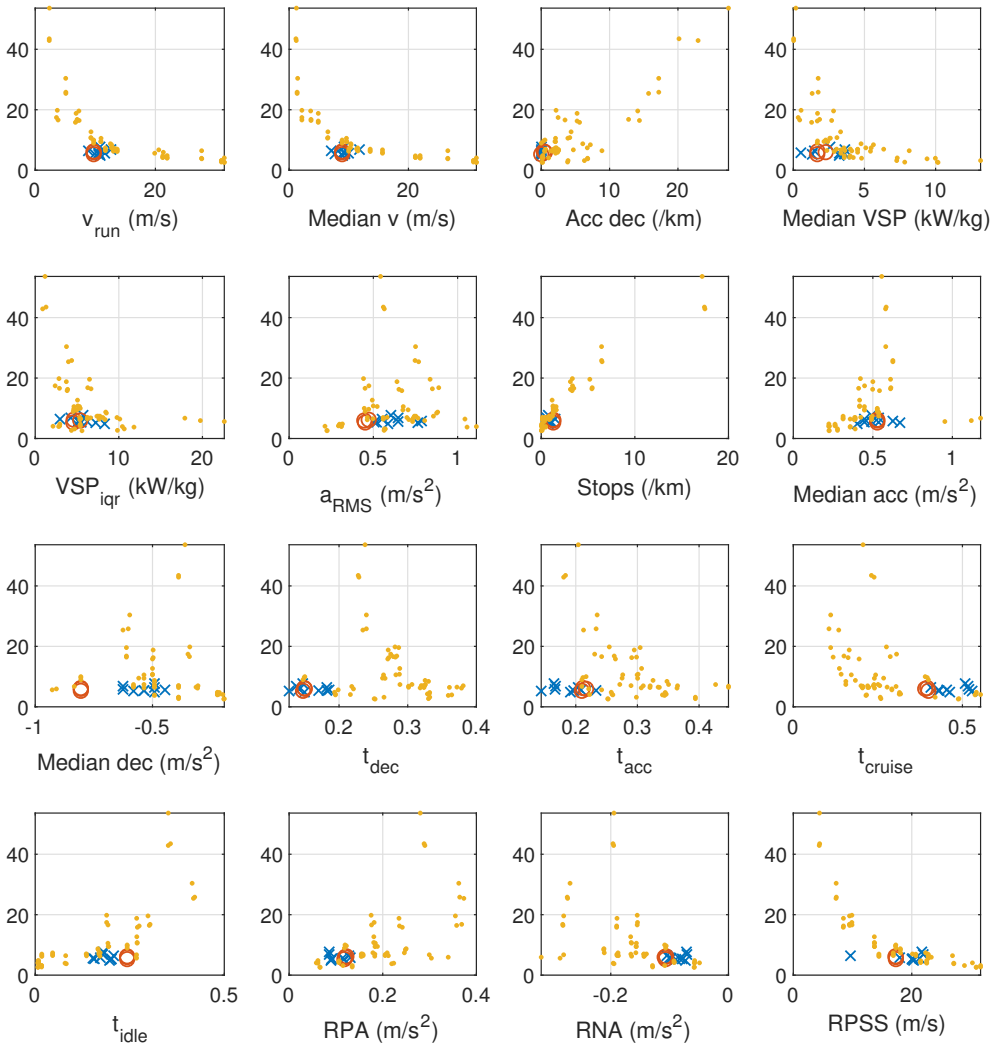

Figure B.14: Scatter plots of fuel economy (l/100 km) against QR predictors for simulated data (yellow dots), training vehicles on the EA PEMS cycle (orange circles) and validation vehicles (blue crosses).

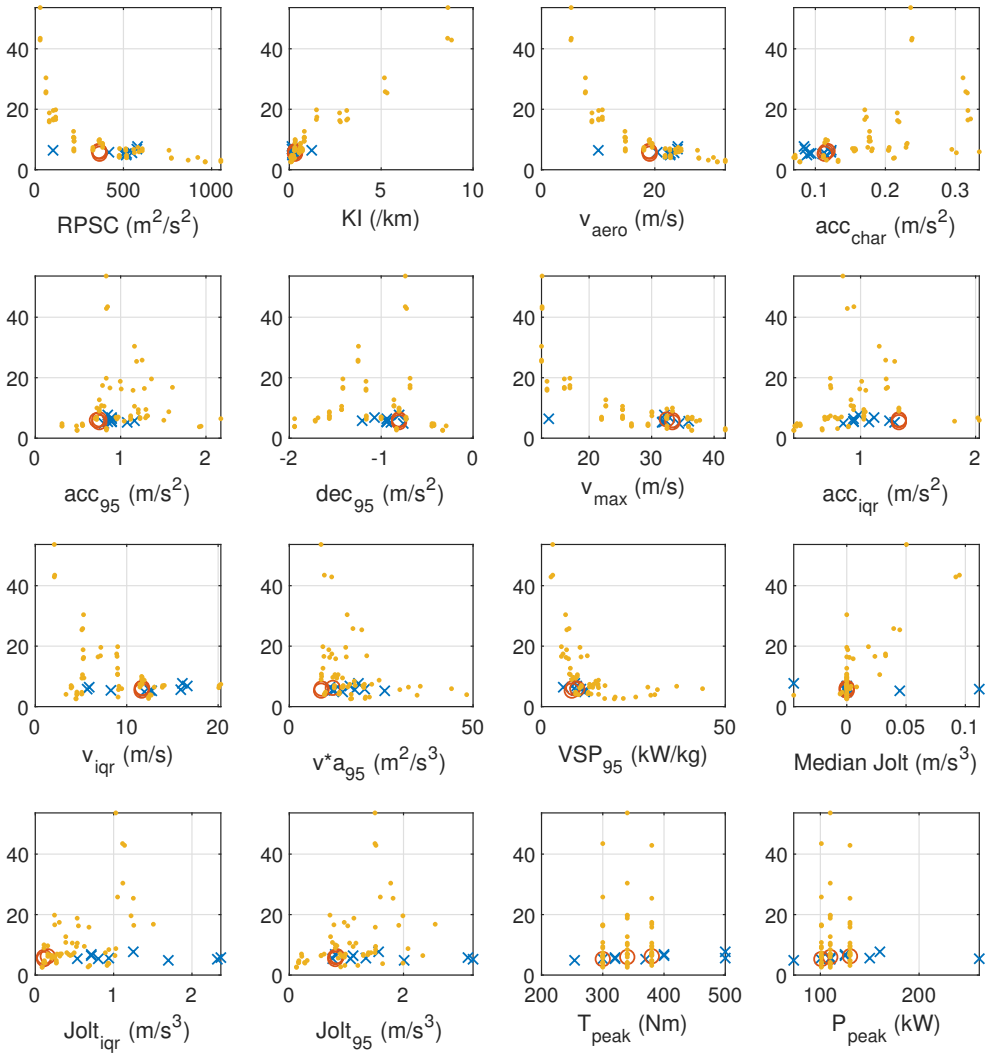

Figure B.15: Scatter plots of fuel economy (l/100 km) against QR predictors for simulated data (yellow dots), training vehicles on the EA PEMS cycle (orange circles) and validation vehicles (blue crosses).

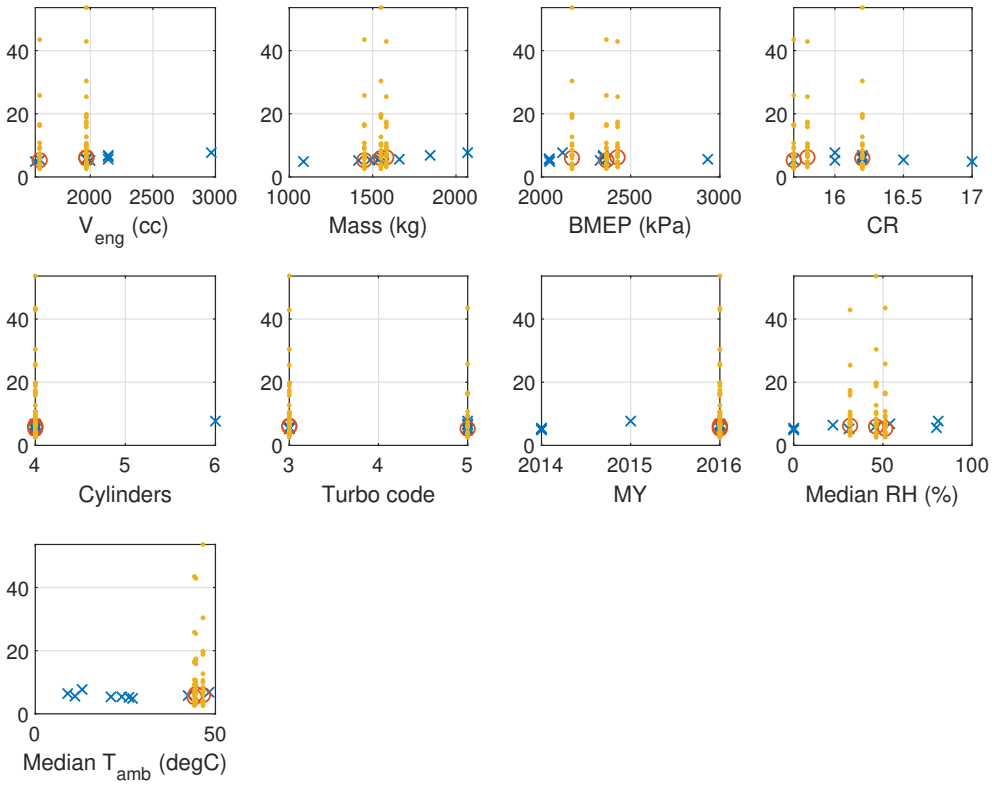

Figure B.16: Scatter plots of fuel economy (l/100 km) against QR predictors for simulated data (yellow dots), training vehicles on the EA PEMS cycle (orange circles) and validation vehicles (blue crosses).

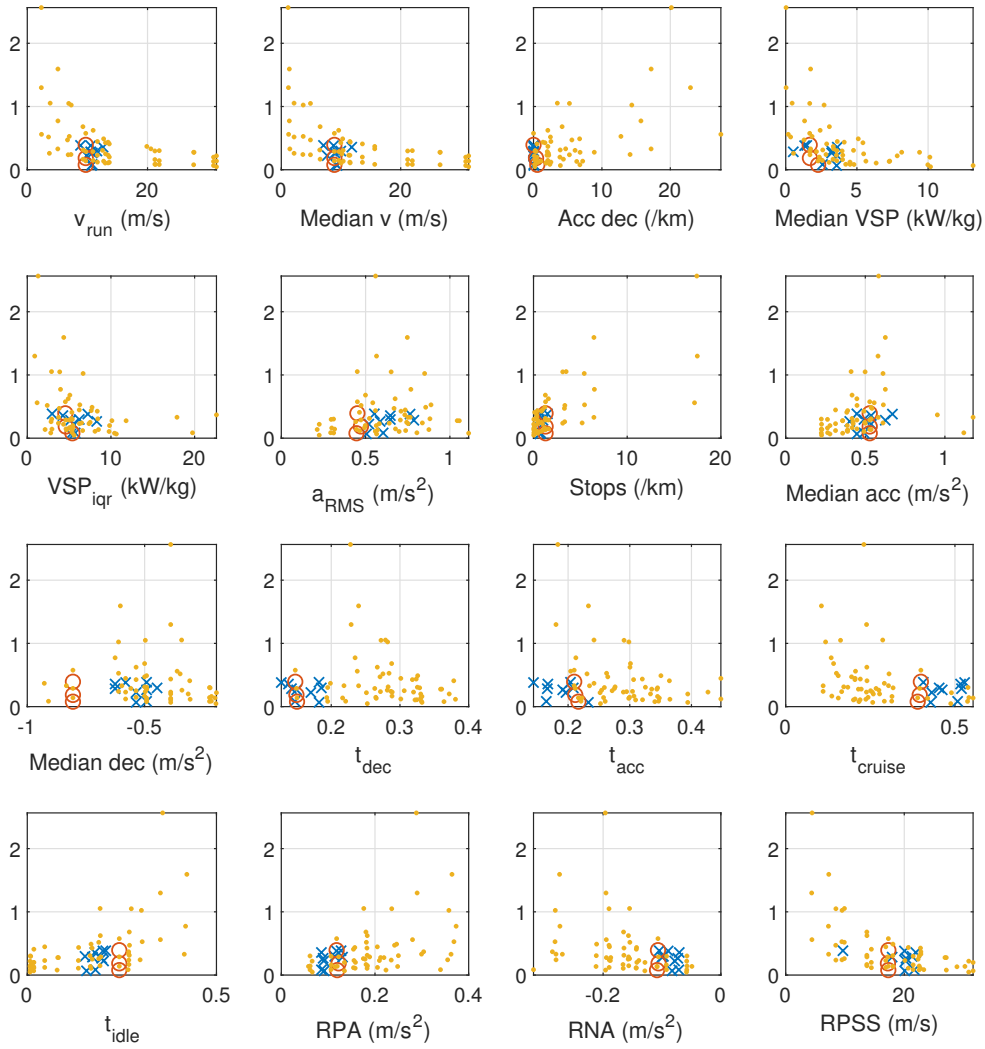

Figure B.17: Scatter plots of NO_x emissions (g/km) against QR predictors for simulated data (yellow dots), training vehicles on the EA PEMS cycle (orange circles) and validation vehicles (blue crosses).

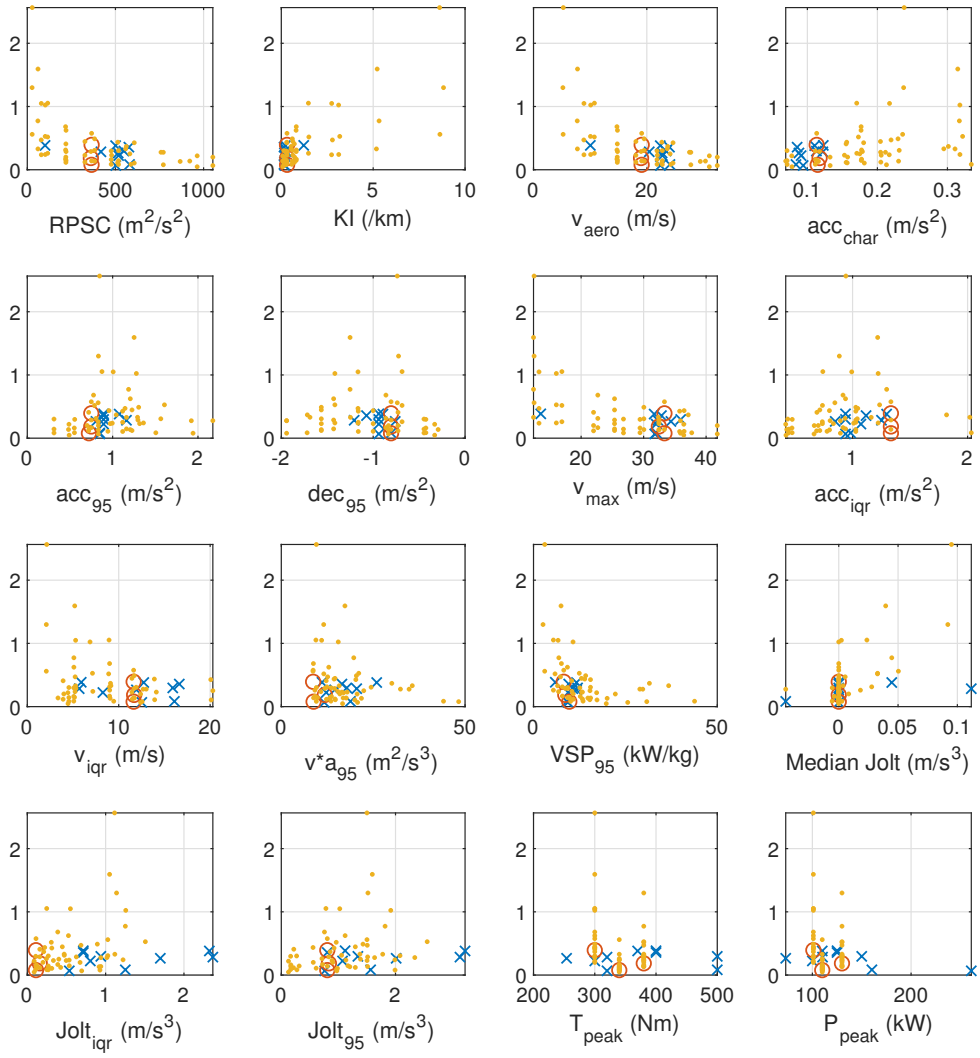

Figure B.18: Scatter plots of NO_x emissions (g/km) against QR predictors for simulated data (yellow dots), training vehicles on the EA PEMS cycle (orange circles) and validation vehicles (blue crosses).

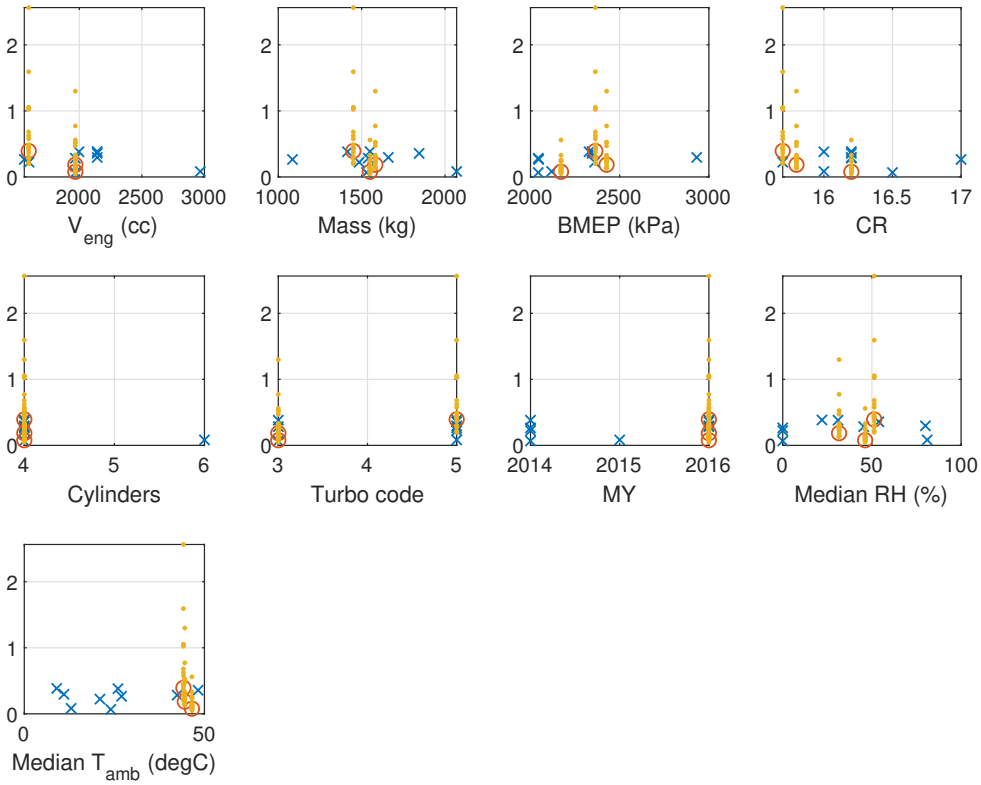

Figure B.19: Scatter plots of NO_x emissions (g/km) against QR predictors for simulated data (yellow dots), training vehicles on the EA PEMS cycle (orange circles) and validation vehicles (blue crosses).

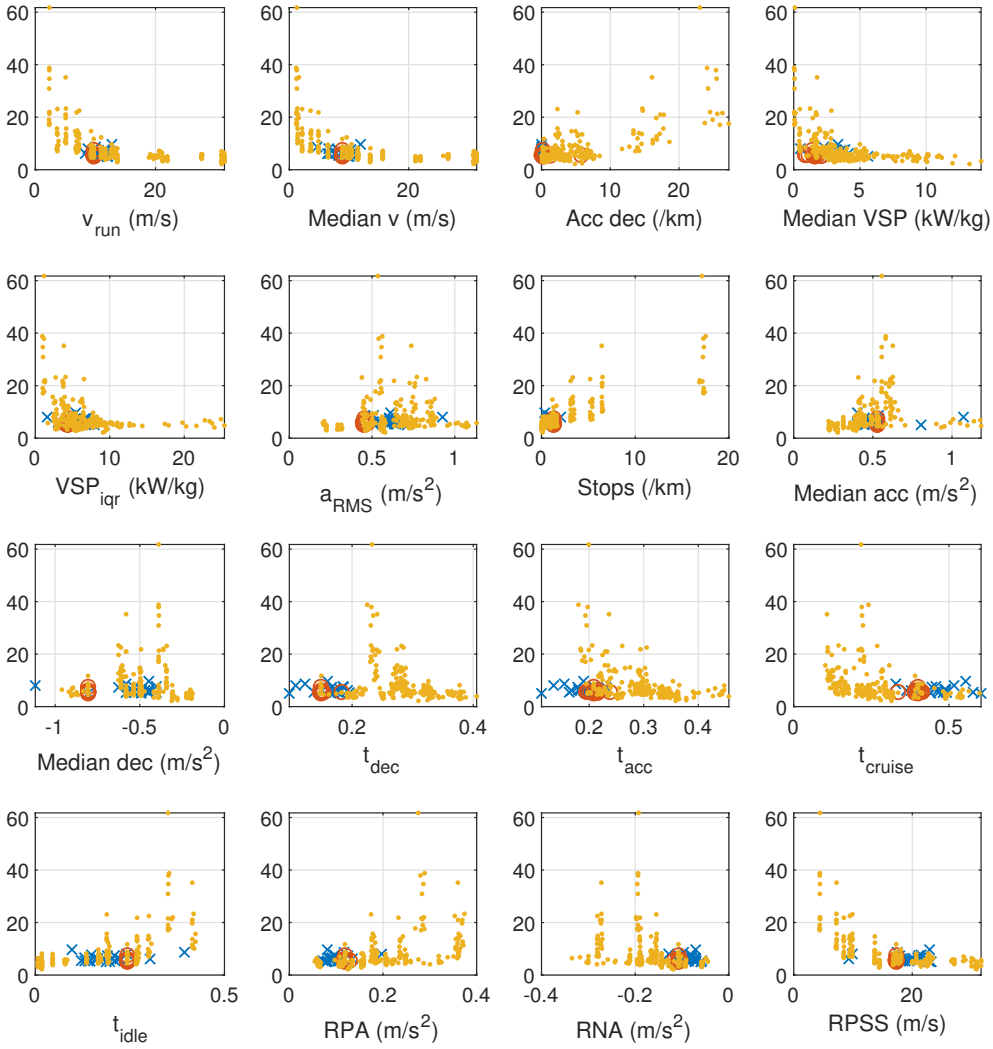

Figure B.20: Scatter plots of fuel economy (l/100 km) against QR predictors for simulated data (yellow dots), training vehicles on the EA PEMS cycle (orange circles) and validation vehicles (blue crosses).

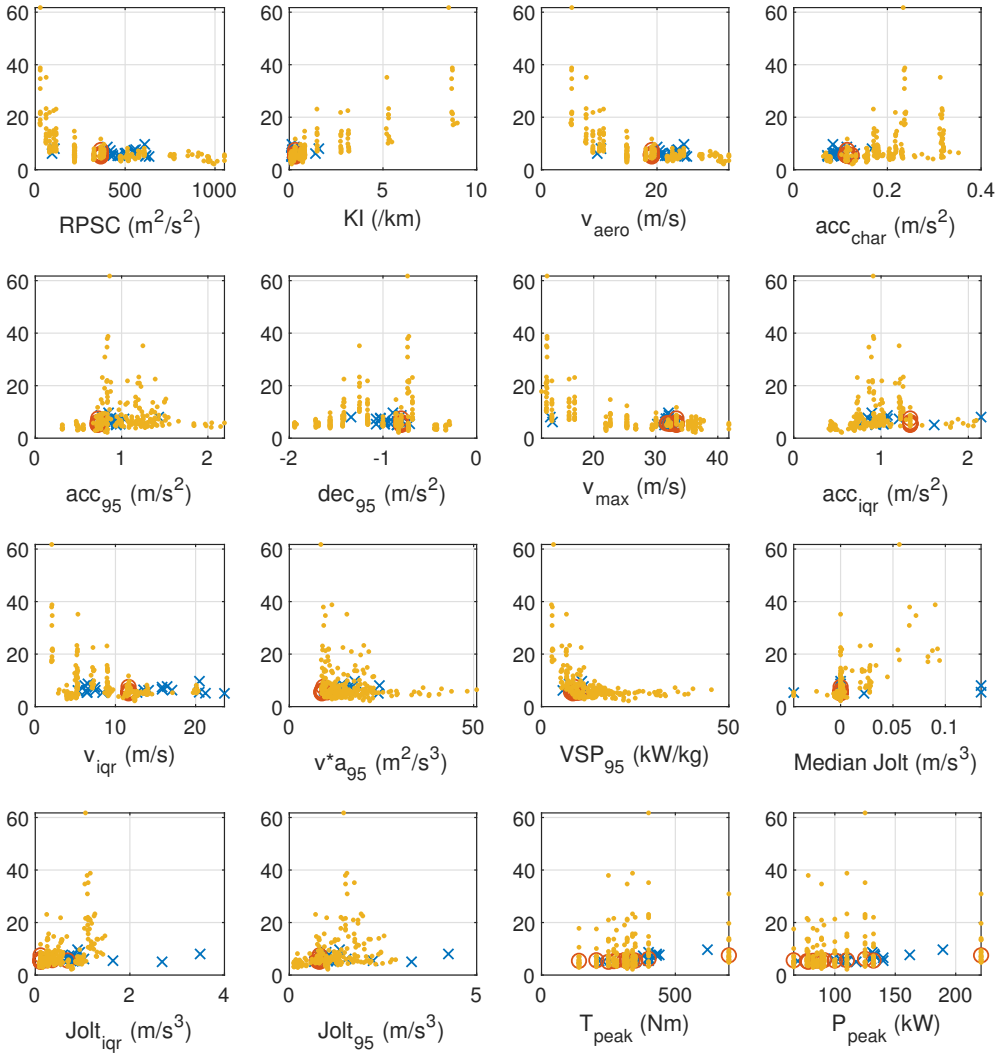

Figure B.21: Scatter plots of fuel economy (l/100 km) against QR predictors for simulated data (yellow dots), training vehicles on the EA PEMS cycle (orange circles) and validation vehicles (blue crosses).

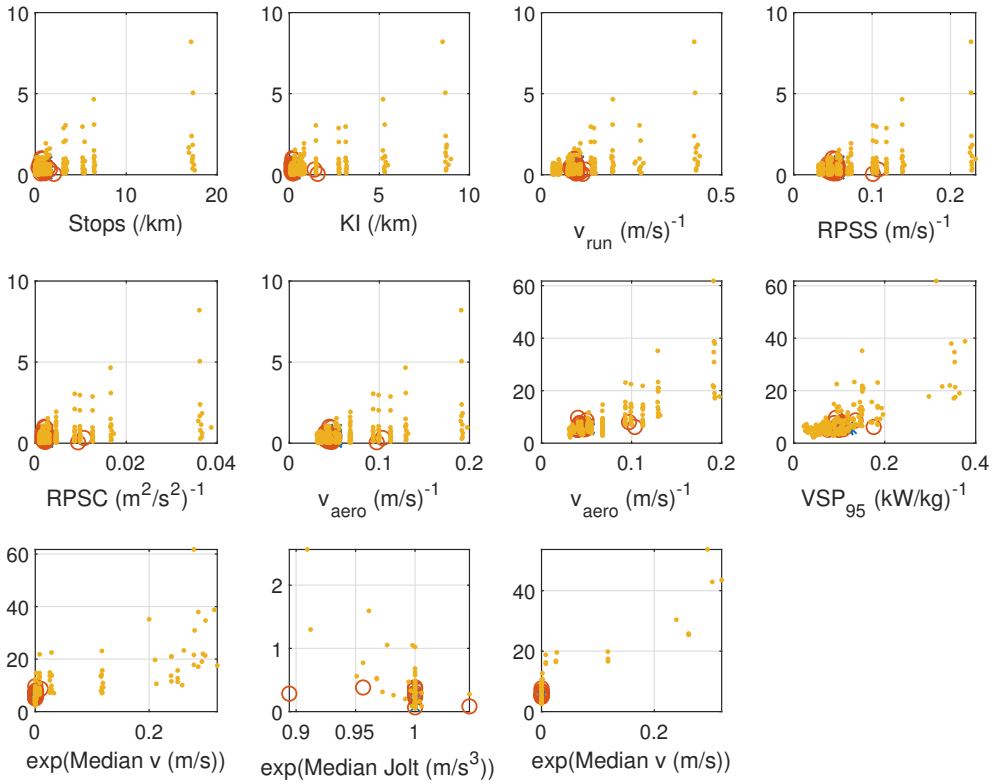

Figure B.22: Scatter plots of fuel economy (l/100 km) against QR predictors for simulated data (yellow dots), training vehicles on the EA PEMS cycle (orange circles) and validation vehicles (blue crosses).

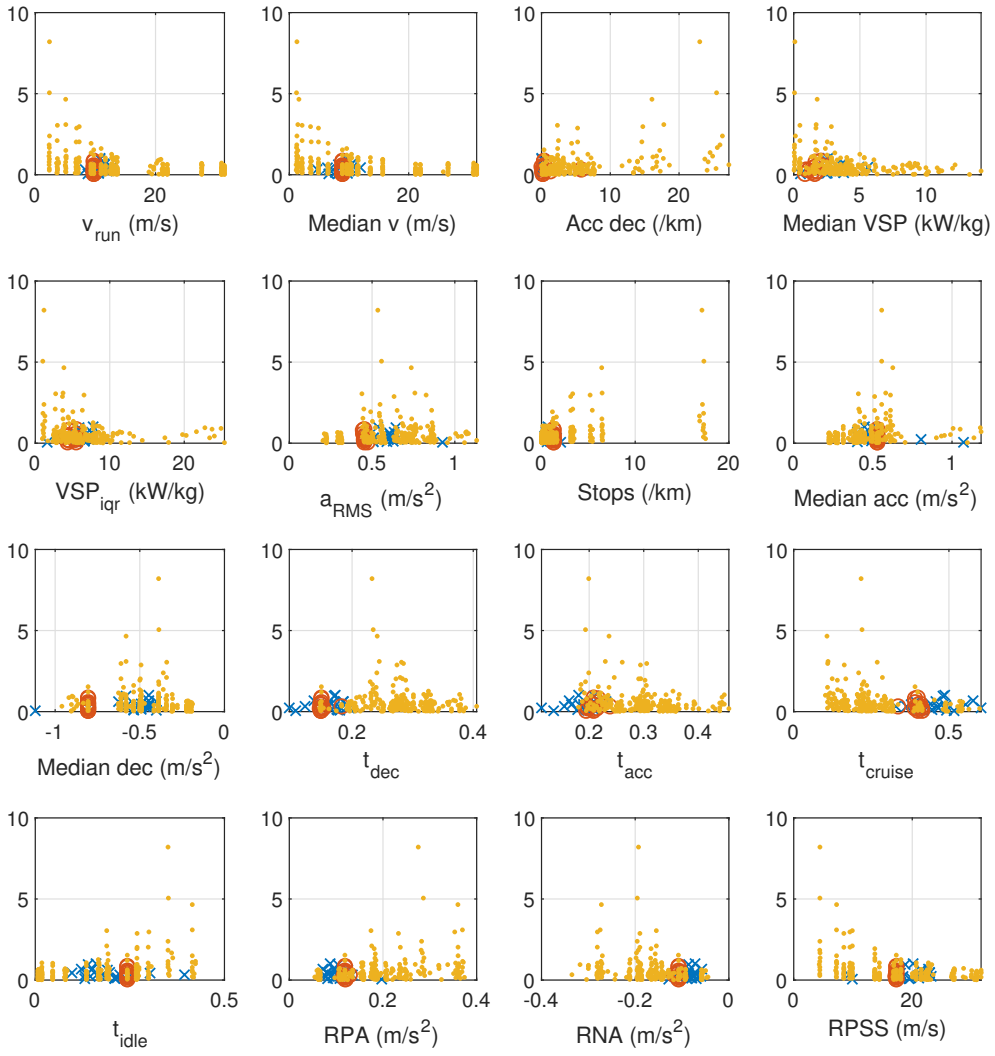

Figure B.23: Scatter plots of NO_x emissions (g/km) against QR predictors for simulated data (yellow dots), training vehicles on the EA PEMS cycle (orange circles) and validation vehicles (blue crosses).

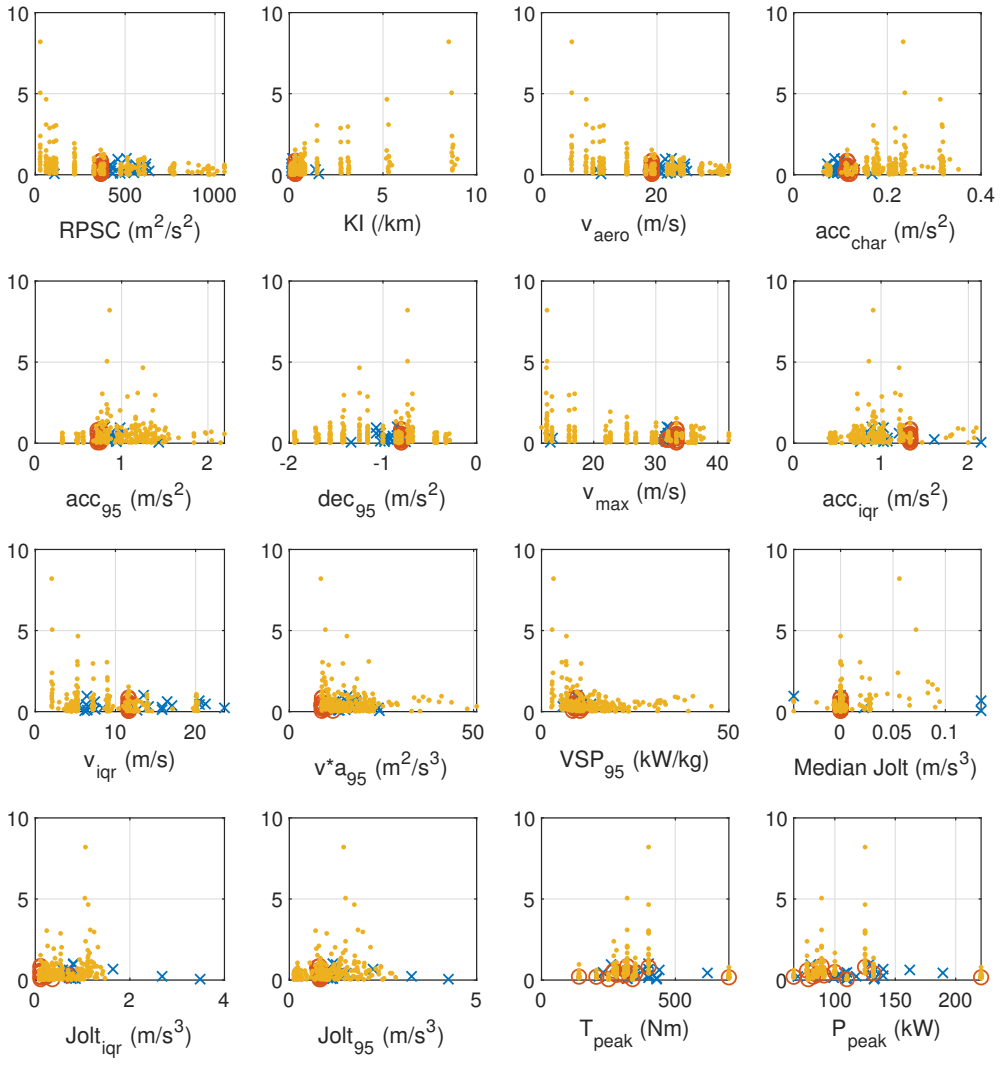

Figure B.24: Scatter plots of NO_x emissions (g/km) against QR predictors for simulated data (yellow dots), training vehicles on the EA PEMS cycle (orange circles) and validation vehicles (blue crosses).

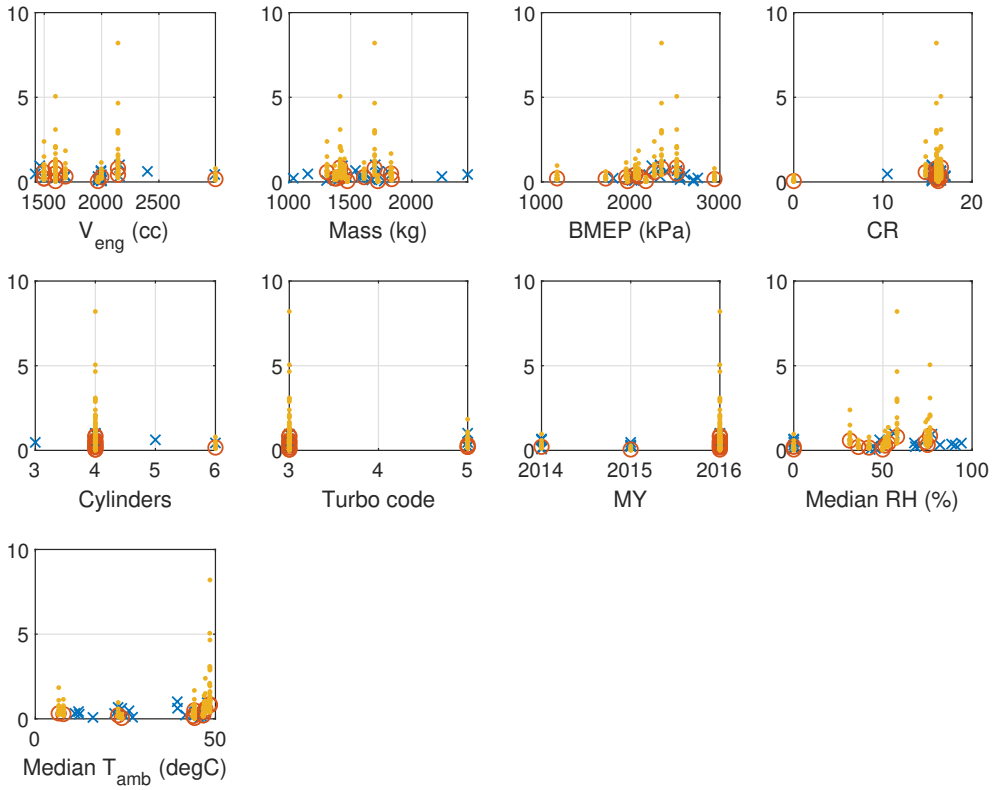

Figure B.25: Scatter plots of NO_x emissions (g/km) against QR predictors for simulated data (yellow dots), training vehicles on the EA PEMS cycle (orange circles) and validation vehicles (blue crosses).